
Wax deposition analysis for oil and gas multiphase flow in pipelines

Aalborg University Esbjerg
Oil and Gas Technology

Master's Thesis



AALBORG UNIVERSITY
DENMARK

Fernando Montero
K10-OG-2-F20

Supervisor:
Rudi Nielsen

June 10, 2020

Contents

Abstract	III
Nomenclature	IV
1 Introduction	1
1.1 Background	1
1.2 Problem statement	2
2 Wax	3
2.1 Wax appearance	3
2.1.1 Wax appearance temperature	3
2.1.2 Pour point	4
2.1.3 Wax content	4
2.2 Wax chemistry	4
3 Wax formation thermodynamics	6
3.1 Phase equilibrium	6
3.2 Thermodynamic models	7
4 Wax deposition via molecular diffusion	9
5 Multiphase flow	11
5.1 Multiphase flow fundamentals	11
5.2 Wax deposition in two phase flow	12
6 Wax deposition Matzain model	14
7 Wax deposition modeling and simulation	17
8 Entry Data	19
8.1 Fluids characterization	19
8.2 Physical properties correlations	20
8.3 Wax precipitation curve	20
8.4 Process conditions and pipeline characteristics	21
8.5 Study cases	21
9 Wax deposition using OLGA[®]	23
9.1 Entry data treatment	23
9.1.1 Fluid characterization	23
9.1.2 Pipeline characteristics	29
9.1.3 Process conditions	30

9.2	Wax deposition simulation setup	30
9.2.1	Discretization independence analysis	31
9.2.2	Stability analysis	31
10	Wax deposition using Matlab®	32
10.1	Entry data treatment	32
10.2	Modeling setup	33
10.2.1	Heat transfer calculations	33
10.2.2	Hydrodynamic calculations	34
10.2.3	Thermodynamic calculations	36
10.2.4	Wax deposition calculations	36
10.2.5	Discretization independence analysis	37
10.2.6	Stability analysis	37
10.2.7	Modeling flow chart	38
11	Results	40
11.1	Heat transfer and fluid mechanics along the pipeline	40
11.1.1	Bulk and wall temperatures	40
11.1.2	Pressure drop profile	44
11.1.3	Superficial velocities	45
11.1.4	Flow pattern prediction	46
11.2	Wax precipitation along the pipeline	47
11.3	Wax deposition	49
11.3.1	Wax deposition profile	50
11.3.2	Wax deposition evolution through time	54
12	Conclusions	58
13	Future work	59
	Bibliography	60
	Appendix	A

Abstract

Wax deposition has been a big challenge for the Oil & Gas industry, and the current energy demand has driven the oil production to remote environments where subsea facilities present low-temperature environments that represent potential financial losses due to wax deposition. Some techniques have been developed to deal with wax formation or deposition problems; however, its modeling and simulation present some limitations related to accurate predictions of wax deposit thickness and location. The closed interrelation of wax deposition process with aspects referring to thermodynamics, heat & mass transfer and fluid mechanics brings additional complexity to wax deposition analysis.

This work consists in a comparative study of modeling and simulation of a subsea horizontal pipeline section transporting a multiphase flow. The analysis is done using a commercial software and a self developed code, which are used to evaluate the prediction of wax deposition using a non-compositional model; always pursuing a better understanding of the wax deposition process, multiphase flow, transport phenomena, and their mathematical models and simulation tools.

Four main cases of analysis are considered in this project in which different gas and liquid mass flow rates are evaluated. Moreover, these four cases are expanded to 16 study cases to include different paraffin characterization and deposition times into the wax deposition analysis. Experimental data available in open literature is used for fluid characterization in both commercial simulator and self developed code.

The results demonstrate the high sensitivity of the wax deposition prediction to the accuracy of the calculation of the inner wall temperature as well as the influence of the thermodynamic approach used in the wax formation analysis.

The wax deposition process is modeled based on the non-compositional Matzain Model through the commercial software OLGA[®] (by Schlumberger) and a code developed in Matlab[®].

Nomenclature

Abbreviations and Initials

API	American Petroleum Institute
ASTM	American Society for Testing and Materials
CapEx	Capital expenditure
CPA	Cubic plus association
CPM	Cross-polarized microscopy
DSC	Differential scanning calorimetry
EoS	Equation of state
FT-IR	Fourier-transform infrared spectroscopy
GUTS	Grand Universal Thermodynamic Simulator
OHTC	Overall heat transfer coefficient
OpEx	Operational expenditure
SRK	Soave-Redlich-Kwong equation of state
UOP	Universal Oil Products company
VLSE	Vapor-Liquid-Solid equilibrium
WAT	Wax appearance temperature

1 Introduction

1.1 Background

Petroleum reservoir fluids are complex mixtures which contain primarily a wide range of hydrocarbons. Most of these fluids contain heavy paraffins which can precipitate and be deposited as a solid-like material namely wax [1].

Wax deposition has been a big challenge for the Oil & Gas industry since its inception; additionally, the current global demand of energy has driven the oil exploration and production to remote environments where avoiding wax deposition requires innovative solutions for cooler and deeper scenarios [2, 3].

Subsea facilities and pipelines are more susceptible to present wax deposition problems during petroleum production due to low-temperature environments and higher heat transfer capacity of these systems surrounded by water [4]. Pipeline operation presents a high risk associated to wax plugging, which worst-case scenario compliance the replacement of a pipe-section or even the abandonment of the production facilities representing high financial losses and environmental problems [5]. In this context, pipeline restarting flow after a programmed or emergency shutdown presents additional attention and challenges related to blockage by gelled waxy crude oil [6, 7, 8].

Pipeline isolation and heating, pipe-in-pipe, wax-repellent surfaces, chemical and biological treatments, mechanical scraping and cold-flow are some techniques useful to deal with wax formation or removal; however, wax deposition modeling and simulation present some limitations related to accurate predictions of wax deposit thickness, location and composition. Indeed, these limitations are frequently observed when real field cases are simulated due to the absence of adequate experimental field data and a strong sensitivity presented by the wax deposition models [9, 10, 11, 12, 13, 14].

The wax deposition process is closely interrelated to other phenomena making difficult its prediction through models and simulations; in other words, factors as the amount, location, composition and hardness of the wax deposited on the inner surface of a pipeline depend on aspects related to thermodynamics, heat & mass transfer and fluid mechanics. Multiphase flow brings additional complexity to wax deposition analysis because parameters as flow regime and superficial phase velocities should be considered [11, 15].

Few studies of wax deposition in multiphase flow have been conducted. Nevertheless, accurate wax deposition predictions are needed to develop reliable and economical solutions to avoid this problem in current more challenging scenarios. Therefore, a good knowledge of the wax deposition process, multiphase flow and transport phenomena involved leads to a better understanding about mathematical models, simulation tools and their optimal setting for real case wax deposition predictions [15, 16].

1.2 Problem statement

The aim of this work is to simulate a horizontal section of a subsea pipeline transporting a multiphase flow from wellhead to offshore production facilities understanding the wax deposition phenomenon. To achieve this objective, the commercial software OLGA[®] (by Schlumberger) and a self developed code are used to evaluate the prediction of wax deposition using a non-compositional model.

For this project, experimental data available in open literature is used. The experimental data related to wax deposition projects considering multiphase flow serves to characterize the fluid for both simulations, acquiring a better knowledge about the interrelation between fluid characterization and wax deposition per se. The model used for the prediction of wax deposition corresponds, in both codes, to the Matzain model.

After model buildup and simulation, a comparative analysis of results is done in order to evaluate the different modules of the code developed in Matlab[®] regarding heat transfer, fluid mechanics and wax deposition.

2 Wax

Basic and general concepts for wax deposition are needed to have a good understanding of the fundamentals linked to this phenomenon. The most important concepts related to wax appearance and its chemistry are presented in this section.

2.1 Wax appearance

Three important concepts should be well understood to have a comprehensive knowledge about wax appearance and related issues. Wax appearance temperature, pour point and wax content give a fundamental basis for wax deposition studies.

2.1.1 Wax appearance temperature

Wax precipitation occurs if paraffin petroleum reservoir fluid is cooled down to the wax appearance temperature (WAT), which is defined as the highest temperature where solid wax molecules start to appear in the reservoir fluid. The term cloud point is also applied, based in a standardized procedure to determine WAT [1, 16, 17].

Different measurement methodologies can be used to determine WAT, but all those give slightly different results due to the applied technique. Some WAT determination examples are the following [1, 18]:

- Microscopic technique is based on the observation of the wax crystals formation, which increase the opacity of the fluid, giving the idea of a *cloud* appearing into the fluid. Standard testing methods, as ASTM-D2500 and ASTM-D3117, can be used for this visual analysis. The cross-polarized microscopy (CPM) uses cross-polarized light to allow the visualization of solid particles in dark oil samples increasing the sensitivity of the standard microscopic technique.
- Differential scanning calorimetry (DSC) is associated to the measurement of heat released by the crystallization wax process. The standard method ASTM-D4419-90 was developed for WAT determination through DSC.
- Fourier-Transform Infrared Spectroscopy (FT-IR) measures the WAT of oil samples based on the distinct IR absorbance of solid wax particles in comparison with the one of liquid oil.
- Wax molecules increase the apparent viscosity of the fluid, so viscometry can be used to determine WAT.

CPM and FT-IR provide the closest values to the exact thermodynamic WAT, whereas DSC and viscosity measure usually result in an estimation of temperature below WAT,

where severe wax precipitation could occur. Regardless the WAT measurement technique, its determination is very important to know under which conditions the wax precipitation starts.

2.1.2 Pour point

The pour point is the lowest temperature at which the oil flows freely under its own weight. This is measured under specific test conditions established by the ASTM D-97 standard. The pour point is considerably lower than the WAT, and crude oils that have significant paraffin content usually present high pour points. During shutdown periods, the temperature can drop below the pour point, making the flow restarting a challenging task. The pour point analysis should be combined with viscosity and yield stress measurements to perform a good rheological fluid evaluation; however, it is a useful rough indicator of flow behavior [1, 19].

2.1.3 Wax content

In a wax precipitation curve (Fig.2.1), the highest temperature represents the wax appearance temperature, where the crystallization of waxy component starts due to cooling. At low temperatures, the precipitation curve usually has an asymptotic trend, which represents the total wax content in oil. The total wax content in an oil can be measured using standards, such as UOP46-64 or UOP46-85 [18]. These standards were developed by the Universal Oil Products company, now Honeywell UOP.

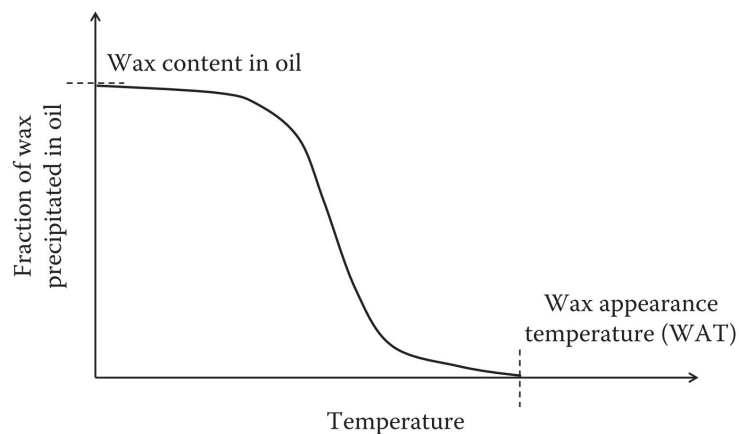


Figure 2.1: Wax precipitation curve [18].

The WAT and wax content are the first two parameters to be checked to determine if wax deposition can be a problem during the production of certain well. Practically speaking, crude oils with more than 2% of wax content and a WAT higher than the subsea floor temperature, which commonly is around 4 °C, can present wax deposition problems [18].

2.2 Wax chemistry

Wax particles are mainly constituted by normal paraffins, but slightly branched paraffins (iso-paraffins) and cycle paraffins (naphthenes) with long paraffinic chains can be found as part of the deposited wax material [1, 16, 17]. Common wax-forming molecules are presented in Fig.2.2.

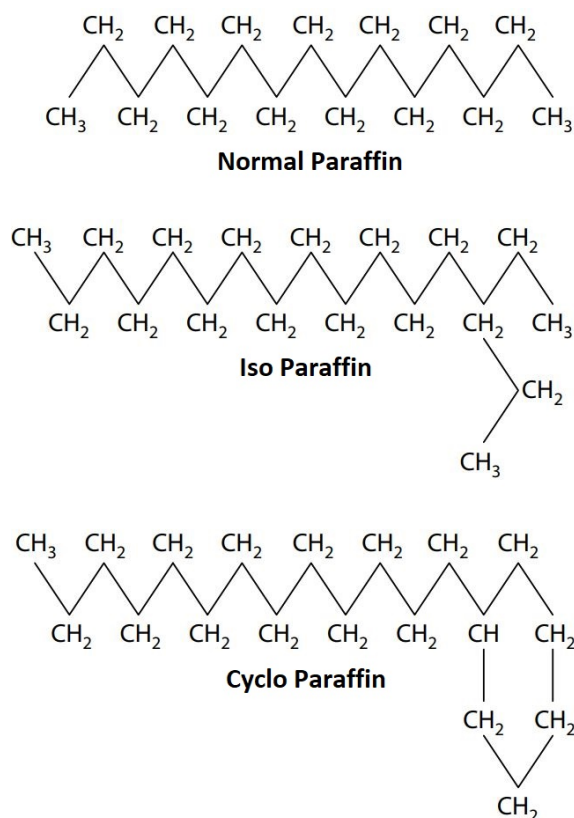


Figure 2.2: Typical wax forming molecules [1].

Regarding wax formation in petroleum reservoir fluids, two types of waxes are defined for crude oils: macro and micro-crystalline wax. Straight-chain n-paraffins in a carbon range from C₂₀ to C₅₀ are mainly present in macro-crystalline wax deposits; on the other hand, branched paraffins and naphthenes in a carbon range from C₃₀ to C₆₀ are dominant in micro-crystalline wax composition. In a fraction with a carbon range higher than approximately C₆₀ the degree of branching is high, making it less likely to be part of the solid structure [1, 17, 20].

Wax deposits related to flow assurance problems consist of around 40-60% of macro-crystalline waxes and less than 10% of micro-crystalline waxes. Additionally, the composition of the deposit varies through time considering that fresh wax deposits present a significant fraction of oil. However, this oil fraction decreases through time making the deposit more solid or harder [17].

The volumetric fraction of the entrapped oil in the deposit is called *wax porosity*. In this concept is assumed that the waxy components are only present in the solid phase and the entrapped oil only consists of non-waxy ones [18]. Porosity is important for both practical and modeling aspects. Through wax porosity analysis the wax removal method to be applied and its frequency can be estimated. In wax deposition modeling, the wax porosity is a parameter which affects wax physical properties and the deposition thickness per se. A common range for wax porosity is from 60 to 90 mass %, corresponding to hard and soft wax deposits, respectively [2, 10, 16, 18, 21].

The wax porosity is also affected by the cooling rate. Higher cooling rates produce softer deposits because the wax is formed and deposited rapidly, entrapping higher oil fractions; on the contrary, lower cooling rates produce harder deposits [16].

3 Wax formation thermodynamics

Wax thermodynamics knowledge is a fundamental part of wax deposition process not only to identify the viability of wax formation but also to determine how severe the deposition could be. However, wax formation analysis is a hard task because the reservoir fluids are complex mixtures, even wax is composed of n-paraffins of different carbon number [18]. A representative phase diagram of waxy oils is presented in Fig.3.1.

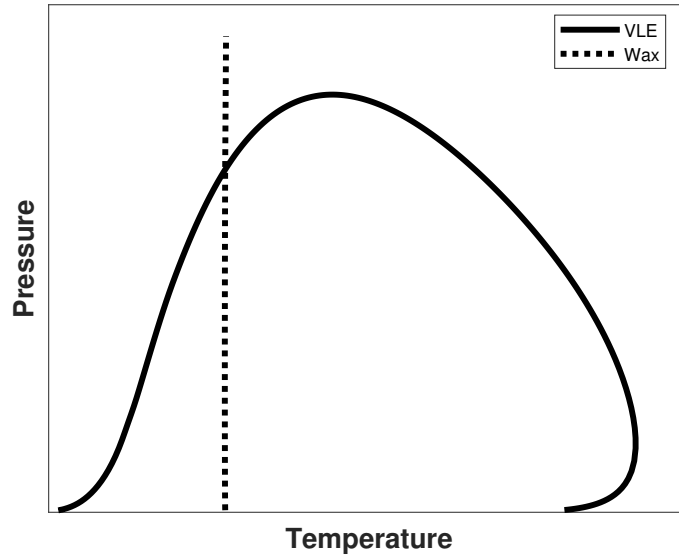


Figure 3.1: Typical phase diagram of waxy crude oil.

3.1 Phase equilibrium

Vapor-Liquid-Solid equilibria are useful to determine the quantity of paraffins dissolved in the liquid hydrocarbon. Describing wax thermodynamics for vapor-liquid equilibrium implies the use of equations of state, as Peng-Robinson, SRK or CPA; however, liquid-solid analysis requires a different approach based on fugacity and Gibbs free energy change [17, 18].

The fugacity of a component i , which represents the tendency of component i to escape from one phase to another. In a Vapor-Liquid-Solid equilibrium (VLSE) the fugacity of component i must be equal in each phase [1, 17, 18]. The fugacity f_i is a function of pressure (P), temperature (T) and molar composition of the different phases (y_i, x_i, s_i).

$$f_i^V(T, P, y_1, y_2, \dots, y_n) = f_i^L(T, P, x_1, x_2, \dots, x_n) = f_i^S(T, P, s_1, s_2, \dots, s_n) \quad (3.1)$$

The phase equilibrium equations (Eq.3.1) together with mass balance (Eq.3.2) and constitutive equations (Eq.3.3) are solved simultaneously to determine the amount of each

phase (n^V, n^L, n^S) and its molar composition (y_i, x_i, s_i).

$$n^V y_i + n^L x_i + n^S s_i = n_i^F \quad (3.2)$$

$$\sum_i^N y_i = 1; \quad \sum_i^N x_i = 1; \quad \sum_i^N s_i = 1 \quad (3.3)$$

3.2 Thermodynamic models

Thermodynamic models are useful tools to predict the solubility of wax components, their fractions in the fluid and the wax concentration [21].

Fugacity and the Gibbs free energy change of a pure liquid compound are used to estimate the corresponding variables for the pure solid. Essentially, the various wax models differ in the way how liquid and solid (wax) fugacities are estimated. Different thermodynamic approaches are used to analyze these non-idealities and calculate the activity coefficients. A general expression which relates fugacity and Gibbs free energy change is shown in Eq.3.4. Depending of the theoretical approach of the analysis, the mathematical form of this equation can vary [1, 18].

$$\ln \frac{f_i^S}{f_i^L} = -\frac{\Delta H_i^f}{RT} \left(1 - \frac{T}{T_i^f}\right) - \frac{1}{RT} \int_T^{T_i^f} \Delta C_{P_i} dT + \frac{1}{RT} \int_T^{T_i^f} \frac{\Delta C_{P_i}}{T} dT + \int_{P_o}^P \frac{\Delta V_i}{RT} dp \quad (3.4)$$

Where ΔH_i^f is the enthalpy of fusion, T_i^f is the melting temperature of component i , ΔC_{P_i} is the difference between solid and liquid state heat capacities at constant pressure for component i , ΔV_i is the difference between the solid and liquid phase molar volume of component i and R is the ideal gas constant.

In addition to non-idealities, two aspects related to phase change from liquid to solid of n-paraffins should be considered. The *secondary phase transition*, which states that the enthalpy for the estimation of the Gibbs free energy, used in Eq.3.4, equals the enthalpy of fusion plus the enthalpy of the secondary phase transition, which is an intermediate stage observed in the solidification phenomenon of n-paraffins. The *equilibrium between multiple solid phases* establishes the coexistence of wax solid phases with different structures (eg. hexagonal and orthorombic) [18].

Some thermodynamic models have been developed to handle wax formation. Different approaches are considered for each model as is shown in Table3.1.

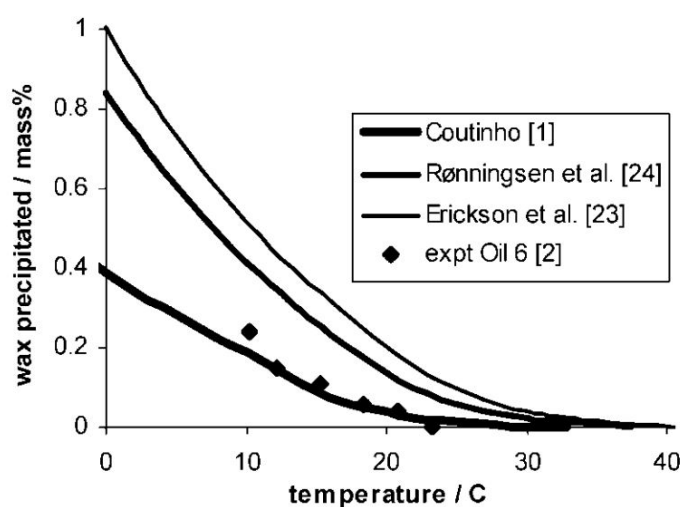
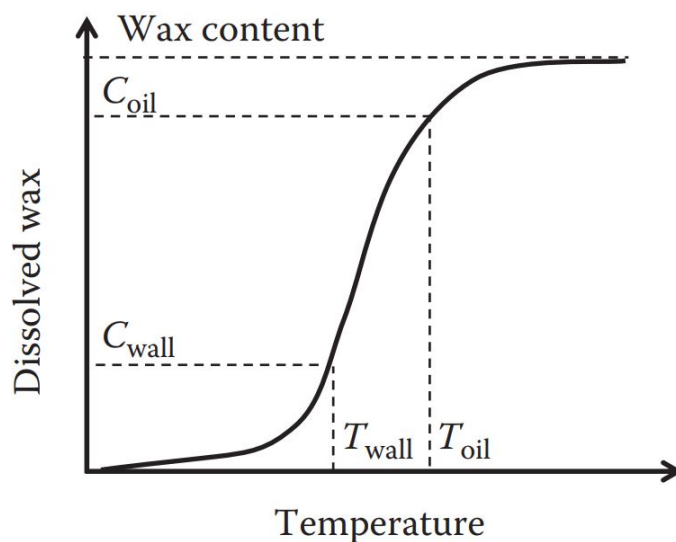
According to literature, Coutinho's model is the most thermodynamically complete method for wax deposition modeling because, in addition to non-idealities for liquid and solid phases, it includes secondary phase transition and multiple solid phases equilibrium [18]. This approach gives to Coutinho's wax model a high accuracy considering experimental data, as is observed in Fig.3.2.

One of the main outputs of thermodynamic analysis of wax deposition is the prediction of the wax solubility curve (Fig.3.3) which can be built inverting the wax precipitation curve. This construction is based on the fact that the amount of dissolved wax is equal to the total amount of wax minus the precipitated one [18].

Considering the radial temperature profile, the corresponding concentrations could be estimated using the wax solubility curve.

Table 3.1: Different thermodynamic models (based on Huang et. al [18])

Model	Liquid non-ideality	Solid non-ideality	Multiple solid phases	Secondary transition	Commercial software
Conoco	–	–	Yes	–	GUTS / LedaFlow
Won's	Yes	Yes	–	–	–
Pedersen's	Yes	Yes	–	–	PVTsim by Calsep
Lira-Galeana's	Yes	–	Yes	–	–
Coutinho's	Yes	Yes	Yes	Yes	Multiflash by KBC

**Figure 3.2:** Thermodynamic models comparison. "Reprinted with permission from [21]. Copyright 2020 American Chemical Society."**Figure 3.3:** Wax solubility curve [18].

4 Wax deposition via molecular diffusion

In a general way, wax deposition occurs in pipeline systems if the temperature of the system is below the WAT, a negative radial temperature gradient is presented by the flow and the surface roughness is large enough to retain the wax crystals [11, 22].

According to literature, the following four wax deposition mechanisms have been proposed: *molecular diffusion* of the dissolved wax molecules, which form waxy components on the inner wall surface; *shear dispersion* of the precipitated waxy particles on the inner surface; *Brownian diffusion* of the precipitated waxy particles on the wall through Brownian motion and *gravity settling* of the precipitated waxy particles towards the bottom of the pipeline. However, as result of several experimental studies, it is widely accepted that molecular diffusion is the dominant mechanism for the wax deposition process; the other mentioned mechanisms have a negligible impact in the wax deposition phenomenon [2, 10, 11, 3, 18].

The wax deposition process throughout molecular diffusion can be explained based on the following description [10, 11, 18]. A scheme of the wax deposition mechanism through molecular diffusion is presented in Fig.4.1.

- **Step 1: Precipitation of dissolved wax**

At temperature values lower than WAT the dissolved wax molecules precipitate forming crystals. This precipitation occurs indistinctly on the bulk of the fluid or on the pipe wall if the local temperature is lower than WAT, but an incipient deposit wax layer is formed on the inner pipe surface.

- **Step 2: Generation of radial concentration gradient**

In normal cooling conditions a negative radial temperature gradient is observed, in other words, the inner wall surface presents a lower temperature than the bulk oil. This makes greater the degree of precipitation on the wall than in the bulk surroundings. Consequently, the concentration of dissolved waxy components is higher in the bulk than on the wall, which is the driving force for the diffusion of wax molecules from the fluid bulk to the inner wall.

- **Step 3: Deposition of waxy components**

The dissolved waxy components that arrive to the wall vicinity precipitate, but now on the surface of the existing deposit increasing its thickness. The molecular diffusion continues if the flow through the pipeline continues as well, resulting in the deposit buildup.

• Step 4: Deposit aging

The deposit aging is a phenomenon in which the solid fraction of wax into the deposit increases, and two main steps describe this phenomenon. The internal diffusion of wax molecules inside the deposit layer increasing the solid wax fraction and the counter diffusion of de-waxed oil out of the deposit, reducing the wax porosity and making harder the remain solid wax layer. However, the aging presents higher rates when the wax deposition process starts because the internal direct and counter diffusion have less resistances in a tinny layer; on the other, the aging process presents an asymptotic trend through the time.

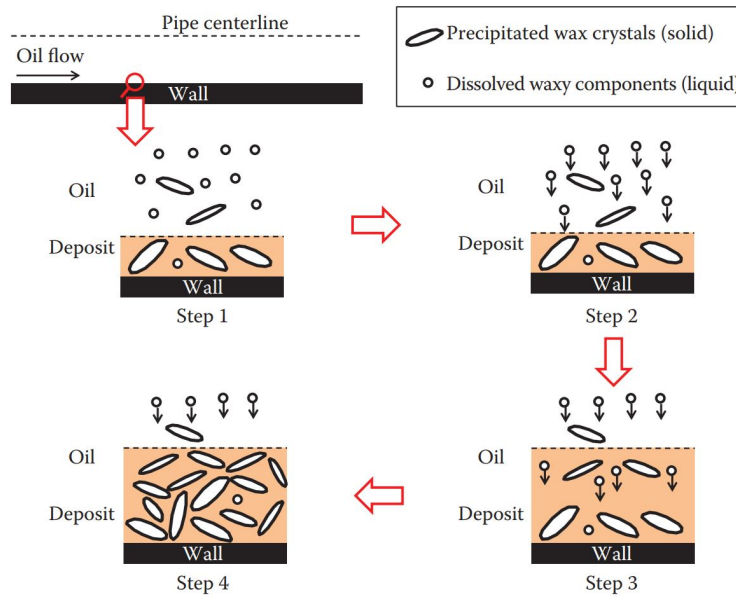


Figure 4.1: Wax deposition through molecular diffusion [18].

Molecular diffusion, described by Fick's Law, can be used as a basis to predict wax deposition rate and tendency [2, 4, 18]. This law can be expressed as a function of the radial temperature gradient as is shown in Eq.4.1.

$$\frac{dm_w}{dt} = -\rho_o D_{wo} A_i \frac{dC_w}{dr} = -\rho_o D_{wo} A_i \frac{dC_w}{dT} \frac{dT}{dr} \quad (4.1)$$

Where m_w is the mass of wax, ρ_o is the density of oil, D_{wo} is the diffusion coefficient of wax in oil, A_i is the inner surface area, C_w is the concentration of wax in oil (weight %), T is the temperature and r is the radial distance (m). .

Nevertheless, Fick's Law cannot solely and correctly predict the wax deposition phenomenon because the wax is a combination of many hydrocarbons and it is not formed by a single component [2].

5 Multiphase flow

Multiphase flow is a common way to transport fluids in the Oil & Gas industry. As was previously stated, petroleum reservoir fluids are complex mixtures which contain a wide range of hydrocarbons. While this fluid is extracted and transported from the reservoir to the surface, the pressure is reduced by the progressive diminution of hydro-static column in vertical pipeline sections and friction losses in horizontal ones. This change in pressure may lead to the appearance of a second phase in the produced fluid [23].

Some concepts have to be defined for a better understanding of the wax deposition process in multiphase flow. Horizontal two-phase flow is reviewed in this section considering that wax deposition models have been developed only based on two-phase flow.

5.1 Multiphase flow fundamentals

The appearance of deformable interfaces is the main characteristic of two-phase flows; and the interfacial distribution is used to classify this flow. Regarding multiphase transport, horizontal flows present more complexity than vertical ones because the gravity tends to segregate the fluid according to density differences [24]. Multiphase flow regimes in horizontal pipelines are commonly divided into stratified, stratified wavy, slug, dispersed bubble and annular flow. A schematic representation is shown in Fig. 5.1.

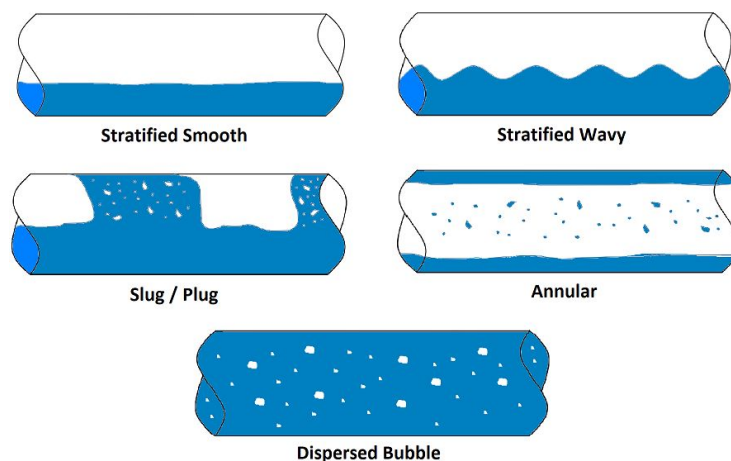


Figure 5.1: Horizontal two-phase flow regimes

In multiphase flow, the portion of area occupied by a particular phase varies in space and time, meaning that the flow is no longer proportional to velocity [23]; however, the superficial velocity concept can be applied when dealing with multiphase flow. The following expressions (Eq.5.1) are used to estimate superficial velocities in two-phase flow.

$$u_{sl} = \frac{Q_l}{A}; \quad u_{sg} = \frac{Q_g}{A} \quad (5.1)$$

Where u_{sl} and u_{sg} are the liquid oil and gas superficial velocities (m/s), Q_l and Q_g are the liquid oil and gas volumetric flows (m^3/s) and A is the pipe cross-sectional area (m^2).

The superficial velocities are useful to predict the flow regime of a multiphase flow under specific conditions. The gas and liquid superficial velocities are plotted along horizontal and vertical axes respectively, creating a flow regime map which help us to identify under which multiphase flow regime the fluid is transported.

An additional parameter to be defined in multiphase flow is the liquid holdup (E), which is the fraction of the area occupied by the liquid phase to the total cross-sectional area of the pipeline.

Several multiphase flow maps have been developed to determine the flow regime based on different parameters. Figure 5.2 shows the flow map presented by Mandhane et al. [25]

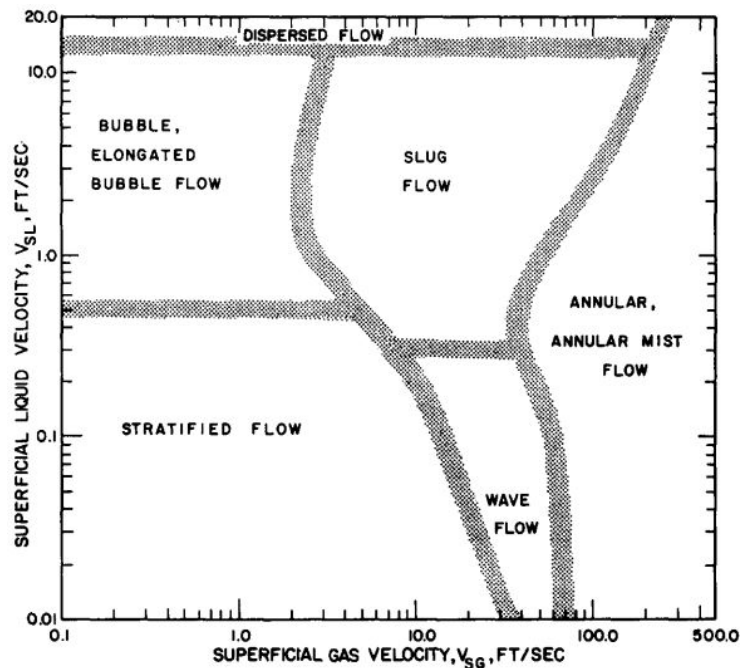


Figure 5.2: Phase flow map - Mandhane [25].

The determination of the flow regime is an important parameter for an accurate prediction of fluid mechanics, heat transfer and even wax deposition phenomena.

5.2 Wax deposition in two phase flow

Wax deposition itself is a complex process which depends on some physical phenomena, making its analysis and prediction a hard task; in addition, when multiphase flow is considered, the number of variables which affect the wax deposition and the process complexity increase.

The multiphase flow regime and phase velocities affect the wax deposit thickness, hardness and profile. For horizontal pipelines, the deposition pattern and thickness varies

according to the flow regime as is shown in Fig.5.3. Wax deposition occurs only in areas where the waxy oil has contact with the surface of the pipeline inner wall [3, 26, 27].

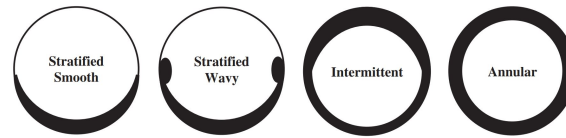


Figure 5.3: Wax deposit distribution - horizontal pipes [3].

Stratified flow presents wax deposition on the lower section of the pipe with a decreasing thickness from the bottom to upward positions. This decreasing behavior is produced due to higher heat transfer rates in the bottom of the pipeline rather than in upward points. The stratified wavy flow deposit has a thicker section along the interface because the waves increase the heat transfer rate. The intermittent flow (slug and bubble) induces higher shear stress on the bottom of the pipeline, resulting in a thinner deposit section on the lower part of the pipe. The annular regime presents a uniform deposition around the pipe if the oil is uniformly distributed over all the pipeline circumference [3, 26, 27].

The deposit hardness is also affected by the flow regime. Stratified and stratified waxy flow present soft deposits at the bottom of the pipe and harder ones on the phase interface. Slug and bubble flow have hard deposits around the pipeline circumference with an increasing hardness trend from the top to the bottom of the pipe. The annular flow presents very hard deposits on all inner surface of the pipe if the oil is uniformly distributed [3, 26, 27].

General observations, made by Matzain et al [27], are shown in Fig.5.4. For horizontal flow the deposit thickness decreases but its hardness increases if the superficial liquid velocity increases. In stratified flow patterns, increasing superficial gas velocity increases the deposit hardness. Under intermittent flow regimes, at higher superficial gas velocity the deposit thickness is increased and its hardness decreased. In the change from intermittent to annular flow regime, only the thickness of the deposit increases [28].

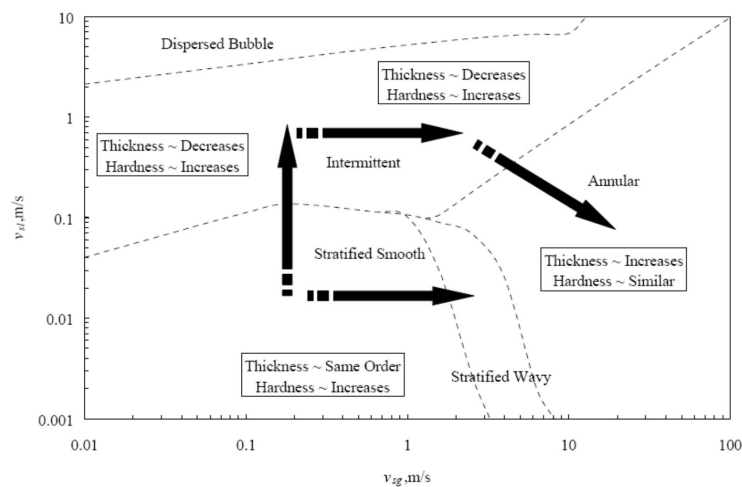


Figure 5.4: Observations in wax deposit - horizontal pipes [26]

Hardness is directly linked to wax deposition management techniques. In other words, the wax removal technique, and its application frequency in pipelines, is mainly established based on the hardness of the deposit.

6 Wax deposition Matzain model

An accurate and reliable prediction of the wax deposition process is required in the Oil & Gas industry to reduce the risk of pipeline plugs and optimize the facilities characteristics and operational procedure in order to reduce expenses related to CapEx and OpEx. So, several mathematical models have been developed through time.

Table 6.1 presents some wax deposition models which are available in commercial software as well in academic programs.

Table 6.1: Different thermodynamic models (based on Huang et. al [18])

Deposition models					
	Matzain, Rygg and Heat Analogy	Lindeloff and Krejbjerg	Edmonds et al.	Hernandez et al.	Huang et al.
Software implementation	OLGA [®] by SLB	DepoWax PVTsim [™] by Calsep	FloWax [™] by KBC	TUWAX by University of Tulsa	MWP by University of Michigan

The models presented in Table 6.1 have the capability to model wax deposition under multiphase conditions. OLGA[®] is the most common transient multiphase simulator in the Oil & Gas industry. TUWAX and MWP are the main academic models which have been developed after decades of research in this flow assurance issue [18].

The following literature review includes the non-compositional Matzain model, which is used in the present project.

The Matzain model is a one-dimensional semi-empirical model based on the molecular diffusion theory, which can be applied to multiphase (gas-oil) flow in pipelines and wellbores. This model incorporates the shear stripping mechanism making possible its application under turbulent and multiphase conditions, where wax removal by shear forces becomes important for an accurate wax deposition prediction [2, 11, 3].

The wax deposition approach for single-phase flow, described in Eq.4.1, is used as a first approximation for wax deposition prediction under multiphase environments. Additionally, this model considers that all the wax that is moved to the wall via molecular diffusion mechanism is deposited on the wall surface. [2].

The net deposition rate is calculated using an empirical modification of Fick's Law (Eq.6.1)

$$\frac{d\delta}{dt} = -\frac{\pi_1}{1 + \pi_2} D_{wo} \left(\frac{dC_w}{dT} \frac{dT}{dr} \right) \quad (6.1)$$

Where δ is the thickness of wax deposited on the inner pipeline surface (m), C_w is the concentration of wax in oil (weight %) and r is the radial distance (m).

D_{wo} , the diffusion coefficient (m^2/s), presented in Eq.6.1, is calculated using the Wilke-Chang correlation (Eq.6.2) [10, 11, 18, 29, 30, 26].

$$D_{wo} = B_{WC} \frac{(\phi_o M_o)^{0.5} T}{\mu_o V_{wax}^{0.6}} \quad (6.2)$$

Where $B_{WC} = 7.4 \times 10^{-12}$, ϕ_o is the oil association parameter (assumed equal to 1), M_o is the oil molecular weight (g/mol), T is the fluid temperature (K), μ_o is the oil viscosity (cP) and V_{wax} is the average molar volume cm^3/mol .

The empirical relation π_1 (Eq.6.3) is related to the rate enhancement due to trapped oil and also accounts for any positive rate not considered by the diffusion constant as turbulent mass diffusion. On the other hand, π_2 (Eq.6.4) accounts for the rate reduction due to shear stripping.

$$\pi_1 = \frac{C_1}{1 - \frac{C_{oil}}{100}}; \quad C_{oil} = 100 \left(1 - \frac{N_{RE,f}^{0.15}}{8} \right), \quad (6.3)$$

$$\pi_2 = C_2 N_{SR}^3 \quad (6.4)$$

Matzian considers that the diffusion coefficient calculated using Wilke-Chang correlation (Eq.6.2) underpredicts the wax deposition phenomenon. C_1 , C_2 and C_3 are three empirical constants which correlate the wax deposition phenomenon between single and multiphase flow. These constants were found to be: $C_1 = 15.0$, $C_2 = 0.055$ and $C_3 = 1.4$ [26].

The empirical constant C_1 attempts to correct the offset in wax deposition prediction considering that flow turbulence enhances the diffusion process via turbulent eddies effect. The empirical constants C_2 and C_3 affect the wax removal due to shear stripping; however, considering that the age of the deposit increases its hardness making more difficult the wax removal, the constants C_2 and C_3 should be changed through time. This feature is not implemented in this model due to the limited understanding about how wax deposit evolves with time [26].

The dimensionless parameter $N_{RE,f}$ (Eq.6.5) is a function of the effective inside diameter related to the wax buildup. In addition, the dimensionless parameter N_{SR} accounts for the limiting deposition effect due to shear stripping, and their expressions were derived for different flow regimes as follows: Eq.6.6 for single-phase flow, Eq.6.7 for stratified and wavy flow, Eq.6.8 for bubble and slug flow and Eq.6.9 for annular flow. All these dimensionless variables are expressed in form of flow regime dependent Reynolds number [26].

$$N_{RE,f} = \frac{\rho_o (v_{sl}) d_{wax}}{\mu_o} \quad (6.5)$$

$$N_{SR} = \frac{\rho_o (v_o) \delta}{\mu_o} \quad (6.6)$$

$$N_{SR} = \frac{\rho_o \left(\frac{v_{sl}}{E} \right) \delta}{\mu_o} \quad (6.7)$$

$$N_{SR} = \frac{\rho_m \left(\frac{v_{sl}}{E}\right) \delta}{\mu_o} \quad (6.8)$$

$$N_{SR} = \frac{\sqrt{\rho_m \rho_o} \left(\frac{v_{sl}}{E}\right) \delta}{\mu_o} \quad (6.9)$$

Where ρ_o and ρ_m are the densities of the oil and oil-gas mixture (kg/m^3) respectively, v_o and v_{sl} are the oil and liquid superficial velocities (m/s) respectively, E is the liquid holdup, d_{wax} is the inside diameter as a result of the wax buildup (m), δ is the thickness of the wax layer (m) and μ_o is the oil viscosity ($kg/(ms)$).

The shear stripping effect is modeled as a function of the deposit thickness, flow conditions and fluid properties, as is shown by all equations developed to estimate the dimensionless parameter N_{SR} (Eqs.6.6, 6.7, 6.8 and 6.9) [11, 29].

The Matzain model calculates the thermal gradient through the laminar sub-layer for deposition by applying Eq.6.10.

$$\frac{dT}{dr} = \frac{T_b - T_{ws}}{k_o} h_{wall} \quad (6.10)$$

Where T_b and T_{ws} are the bulk fluid and wax deposit surface temperature (K) respectively, k_o is the oil thermal conductivity ($W/(mK)$) and h_{wall} is the inner wall heat transfer coefficient ($W/(m^2K)$).

An apparent weakness of the Matzain model lies on that all the experimental work developed for its construction only uses oil from South Pelto block. However, many studies recognized this model as the most accurate one for wax deposition prediction after an adequate tuning [10, 11, 12, 29, 31].

7 Wax deposition modeling and simulation

Wax deposition analysis in the Oil & Gas industry requires different input sources due to its complexity, for instance laboratory analyses, experimental and field data, to obtain adequate management strategies to face wax deposition issues.

As seen in Fig.7.1, experimental data regarding wax formation is a useful tool to tune the thermodynamic wax deposition model. A valuable output of this model is the solubility curve, which at the same time, is an input of the wax deposition modeling. Commonly, wax deposition modeling needs experimental data, required to obtain an accurate prediction of this phenomenon. As a result of a correct wax deposition modeling, an accurate prediction of wax deposition growth considering field conditions can be used to have good management strategies [18].

It is important to notice that high-quality and specialized experimental data is needed to match the results of the modeling with the real field data, and consequently, obtain accurate predictions [10, 11, 12, 13, 14].

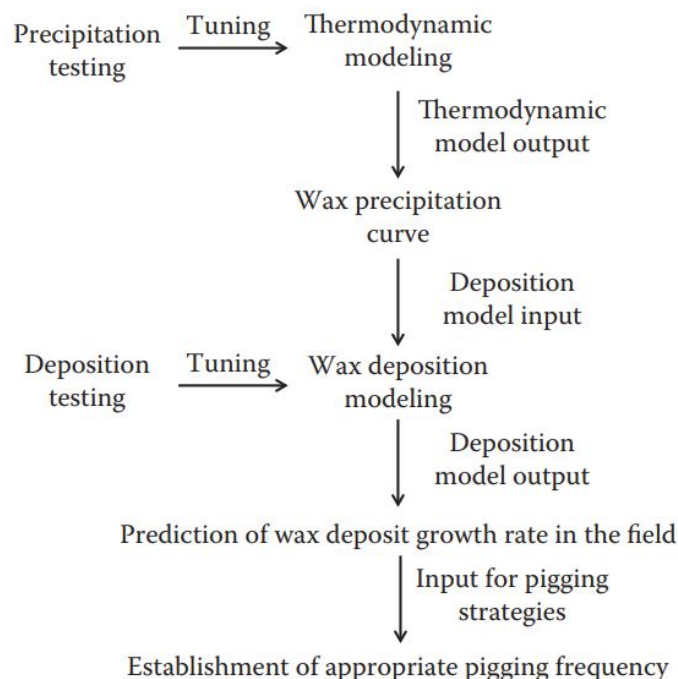


Figure 7.1: General overview of wax modeling [18].

Regarding specifically to wax deposition modeling, Fig.7.2 summarizes a general algorithm, from where it is easy to see that wax deposition is coupling of multiphase fluid

flow, VLSE thermodynamics, multiphase heat transfer and mass transfer [2].

For the hydrodynamic and heat transfer calculations, operating conditions, pipeline characteristics and fluid properties are needed, obtaining the bulk temperature profile of the pipeline and the corresponding pipe wall temperatures. These profiles along with the wax solubility curve are used as input for the mass transfer module (wax deposition mechanism). Altogether, the algorithm results in the determination of the wax deposit growth [18].

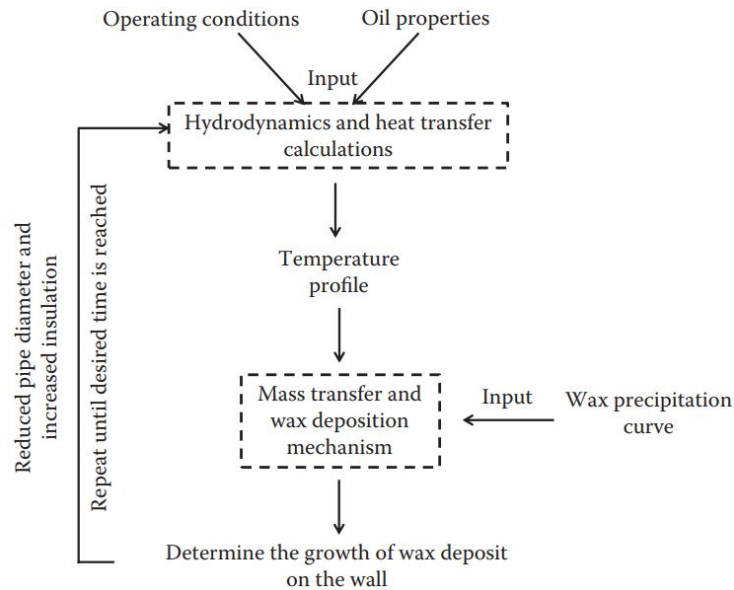


Figure 7.2: General algorithm for wax deposition modeling [18].

The deposit buildup, not only reduces the effective diameter of the pipe, but also increases the heat transfer insulation; thus, heat transfer and hydrodynamic calculations must be continuously updated for the application of the algorithm.

This project is divided into two main analyses. The first one simulates and models the wax deposition phenomenon using OLGA[®] which is a commercial code owned by Schlumberger. The second approach corresponds to the use of a simplified code developed in Matlab[®] to simulate wax deposition to further perform a comparative analysis. Both analyses use the same fluid-related data available in open literature to evaluate the wax deposition phenomenon.

8 Entry Data

This section shows the experimental data regarding pipeline characteristics, fluid composition and properties and special input data needed for wax deposition modeling.

The aim of this work is to get a better understanding regarding wax deposition phenomenon and its modeling. For this reason, simulations using OLGA[®] and Matlab[®] are performed based on experimental data available in literature.

The experimental data for the present work is sourced from Chi [15] and Rittirong [28], both projects from Tulsa University. The information available in the cited works is used for fluid characterization while some process conditions and pipeline characteristics are taken from some typical industry values presented by Gudmundsson [17] and Bai [4].

8.1 Fluids characterization

Tables 8.1, 8.2 and 8.3 show the entry data related to the liquid phase, which corresponds to Garden Banks condensate (GBC) production.

Table 8.1: General properties of GBC [15]

Parameter	Symbol	Units	Value
Wax content	–	wt%	4.3
API gravity	–	°API	42.1
Wax appearance temperature	WAT	°C	35.55

Table 8.2: Single carbon number composition of GBC [15, 28]

Component	wt %						
C5	0.43	C16	4.14	C27	1.49	C38	0.90
C6	1.43	C17	2.96	C28	1.45	C39	0.63
C7	3.40	C18	3.37	C29	1.48	C40	0.84
C8	5.88	C19	3.74	C30	1.34	C41	0.56
C9	6.11	C20	2.58	C31	1.23	C42	0.52
C10	5.80	C21	2.46	C32	1.45	C43	0.47
C11	5.44	C22	2.31	C33	1.30	C44	0.51
C12	4.47	C23	2.17	C34	0.70	C45	0.94
C13	4.80	C24	1.92	C35	0.95	C46	0.26
C14	5.17	C25	1.76	C36	0.91	C47	1.05
C15	3.40	C26	1.71	C37	0.74	C48+	4.81

Table 8.3: n-alkane analysis for GBC [15, 28]

Component	wt %						
C5	0.2036	C16	0.6019	C27	0.0976	C38	0.0124
C6	0.7285	C17	0.4992	C28	0.0678	C39	0.0120
C7	1.2544	C18	0.4290	C29	0.0630	C40	0.0099
C8	1.4204	C19	0.4694	C30	0.0642	C41	0.0121
C9	1.3588	C20	0.3521	C31	0.0562	C42	0.0073
C10	1.2131	C21	0.2905	C32	0.0488	C43	0.0088
C11	1.0843	C22	0.2464	C33	0.0398	C44	0.0098
C12	0.9457	C23	0.1839	C34	0.0376	C45	0.0090
C13	0.8632	C24	0.1808	C35	0.0306	C46	0.0037
C14	0.7275	C25	0.1825	C36	0.0225	C47	0.0039
C15	0.7886	C26	0.1143	C37	0.0188		

Table 8.4 shows the entry data related to the gas phase, which corresponds to natural gas provided by Oklahoma Natural Gas Company (ONG). The average molecular weight of the gas phase (MW_g) is 17.68 [15, 28].

Table 8.4: Natural gas composition [15, 28]

Compound	wt %
Methane	84.5
Ethane	6.5
Propane	4.0
Butane	2.5
Pentane	1.5
Hexane	0.5
CO ₂	0.5

8.2 Physical properties correlations

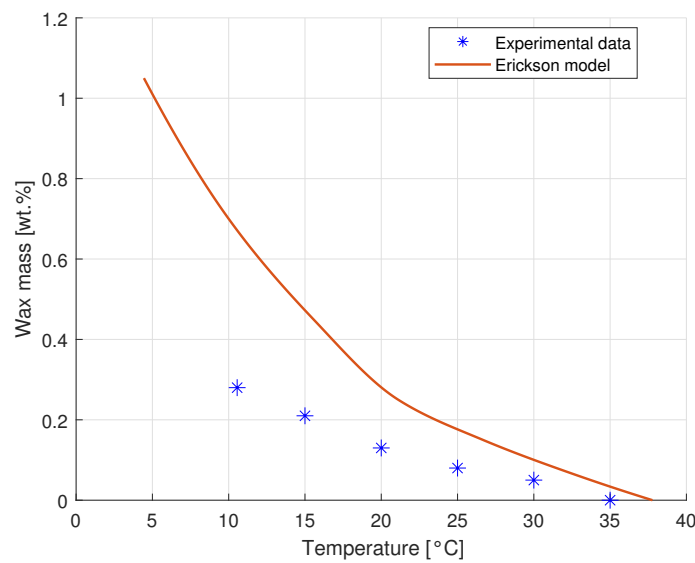
Some physical properties are estimated using given specific correlations as function of temperature (Table 8.5), according to the information provided by Chi and Rittirong [15, 28]. Note that temperature is expressed in degree Fahrenheit ($^{\circ}\text{F}$) in the aforementioned correlations, and the gas density correlation corresponds to pressure values of 2.51 MPa, which is the operating pressure used by Chi and Rittirong.

8.3 Wax precipitation curve

The wax precipitation curve represents the amount of solids precipitated from the fluid mixture as a function of temperature. Figure 8.1 presents the experimental data regarding wax formation collected by differential scanning calorimetry (DSC) as well as the wax precipitation curve estimated through Erickson's thermodynamic model according to the information provided by Rittirong [28].

Table 8.5: Physical properties correlations [15, 28]

Parameter	Symbol	Units	Correlation
Liquid oil			
Density	ρ_o	kg/m^3	$\rho_o = -3.9630E - 01(T) + 8.5861E + 02$
Thermal conductivity	k_o	$W/(mK)$	$k_o = -2.9980E - 04(T) + 2.0954E - 01$
Heat capacity	Cp_o	$J/(kgK)$	$Cp_o = 2.0819(T) + 1885.8$
Interfacial tension	σ	mN/m	$\sigma = -0.0157(T) + 17.6660$
Gas			
Density @ 2.51 MPa	ρ_g	kg/m^3	$\rho_g = -4.30023E - 02(T) + 2.23029E + 01$
Thermal conductivity	k_g	$W/(mK)$	$k_g = 5.9630E - 05(T) + 3.2221E - 02$
Heat capacity	Cp_g	$J/(kgK)$	$Cp_g = 0.8298(T) + 2282.2$

**Figure 8.1:** Wax weight fraction (based on [28])

8.4 Process conditions and pipeline characteristics

The main characteristics of the pipeline as well as the conditions of the process used for the modeling and simulation of wax deposition phenomena are shown in Table 8.6.

The wax deposition analysis for this section uses typical values for process and pipeline characteristics, which are reported by Gudmundsson [17] and Bai [4].

8.5 Study cases

Based on the experimental data, four main cases are analyzed using OLGA[®] and Matlab[®], as presented in Table 8.7. These cases are defined considering different liquid and gas mass flows, according to some study cases presented by Chi and Rittirong [15, 28]. The aforementioned cases are also used to validate the multiphase flow pattern prediction module developed in Matlab[®].

In order to evaluate the effect of time in the wax deposition phenomenon, each case is run considering two deposition times: 10 and 30 days, obtaining in total 8 cases of analysis. In

Table 8.6: Pipeline characteristics [4, 17]

Parameter	Symbol	Units	Value
Process parameters			
Inlet temperature	T_{in}	$^{\circ}\text{C}$	60
Ambient temperature	T_{amb}	$^{\circ}\text{C}$	5
Outlet pressure	P_{out}	MPa	2.51
Pipeline characteristics			
Nominal pipe diameter	d	in	40
Pipe wall thickness	–	in	1
Inner pipe material	–	–	Carbon Steel
Pipe thermal conductivity	k	$\text{W}/(\text{mK})$	45
Pipe roughness	ϵ	m	$4.572E - 5$
Pipe length for evaluation	L	km	20

the name of each case, E stands for experimental data that is used in the present project.

Table 8.7: Main study cases based on experimental data [15, 28]

Case	Liquid flow	Gas flow
	kg/s	kg/s
1E	32.49	11.14
2E	32.49	22.29
3E	591.35	11.14
4E	591.35	44.58

9 Wax deposition using OLGA[®]

This section presents the methodology used in the entry data treatment and simulation setup for wax deposition analysis using OLGA[®].

9.1 Entry data treatment

The important parameters required as input data for OLGA[®] simulator are fluid characterization, process conditions and pipeline characteristics.

9.1.1 Fluid characterization

The fluid characterization is done through Multiflash[®], which is a tool available in OLGA[®]. Multiflash[®] works as a fluid characterization environment, where different files are generated. Such files are later read by OLGA[®] to determine the properties of the fluids involved in the simulation.

The information available in the work done by Rittirong [28] is used in the fluid characterization made in Multiflash[®]. The oil API density, single carbon number (SCN) composition of the oil and n-alkane analysis, presented in Tables 8.1, 8.2 and 8.3, are introduced in the Single Fluid and N-Paraffins (STO) characterization option of the PVT Analysis module as basic information needed for Multiflash[®] to perform the fluid characterization. Figure 9.4, presented ahead in this section, represents the workflow followed for the oil characterization in Multiflash[®].

The carbon number distribution obtained through Multiflash[®] is presented in Fig.9.1. The trend followed by the calculated carbon number distributions looks acceptable considering the experimental data scatter according to the plot presented in Fig.9.1.

It is important to note that Multiflash[®] generates tables for flash calculations and wax formation considering fluid characterization, equation of state, thermodynamic wax model and pressure-temperature conditions. These tables are used in the calculation of wax deposition simulations performed by OLGA[®]. However, the wax appearance temperature (WAT) estimated by Multiflash[®] can be done considering two possible analyses: CPM and DCS with 0.045 wt% and 0.3 wt% of wax as the minimum precipitation criterion to determine the WAT, respectively. On the other hand, OLGA[®] takes the first point of the wax precipitation curve, which corresponds to a criterion of 0.0 wt% of wax, as the WAT of the fluid. A lower wax precipitation criterion results in a higher WAT; in other words, the WAT used by OLGA[®] is higher than the WAT calculated by Multiflash[®]. This difference leads to analyze an additional characterization in which the paraffin composition has been modified in order to match the experimental fluid WAT (35.5 °C) and the value reported by OLGA[®].

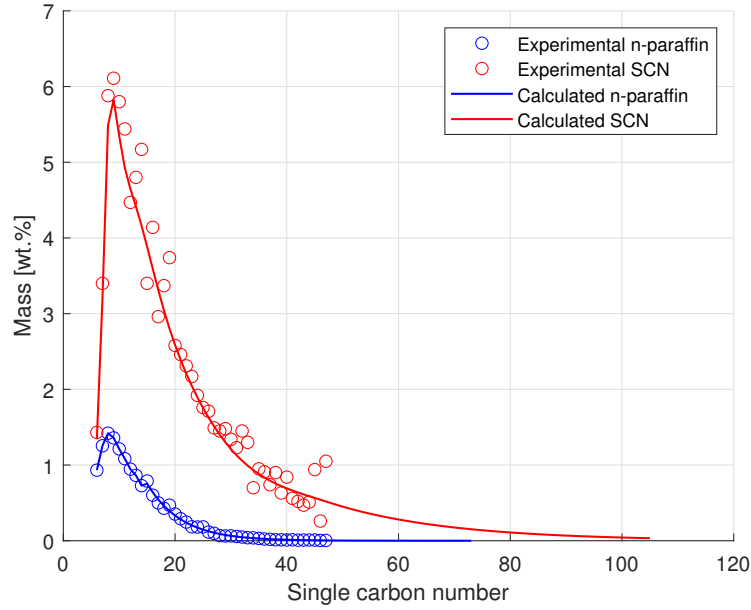


Figure 9.1: Fluid characterization performed in Multiflash[®]

Therefore, the four main cases presented in Table 8.7 are expanded to 16 cases, which are shown in Table 9.5, considering that each case is run for two deposition times (10 and 30 days); and additionally, each case is analyzed using two paraffin compositions, the first one using the information presented in Table 8.3, and the second one based on a modified wax composition done to match the WAT of 35.5 °C (308.65 K) in OLGA[®].

Modified wax composition

The wax composition of the fluid presented in Table 8.3 is modified by maintaining constant the total mass of wax. In addition, the model presented by Pedersen et. al [1] (Eqs.9.1 and 9.2) for plus fraction characterization is used for the wax composition modification.

$$SCN = A + B \ln(z_{SCN}) \quad (9.1)$$

The constant coefficients A and B are obtained through a linear regression of SCN and the logarithm of the corresponding composition.

The mass balance must be closed, which means the summations of wax composition of each carbon number must be equal to the total wax reported in the original n-alkanes composition (14.77 wt%), as is presented in Eq.9.2.

$$z_W = \sum_{i=C_o}^{C_{max}} z_i \quad (9.2)$$

The aim of this modification is based on obtaining a wax composition that presents a wax appearance temperature (WAT) of 35.5 °C in OLGA[®]; for this, a reduction in the wax content of heavy fractions is needed. Thus, a trial and error analysis is done splitting the original composition in three sections (C11-C22, C23-C34, C35-C47). Eq.9.1 is applied to each section, obtaining a new wax composition; always verifying that the total amount of wax be equal to the original amount (14.77 wt%). The initial value of each section presents the corresponding value of the original composition. Table 9.1 shows the constant coefficients (A and B) for each section.

Table 9.1: Constant coefficient for modified wax composition

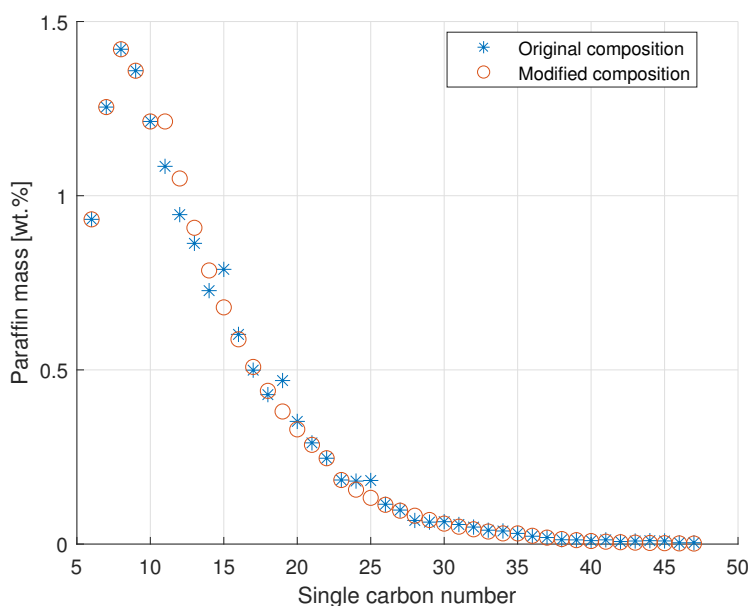
Section	A	B
C11 - C22	-6.90	12.33
C23 - C34	-6.13	12.61
C35 - C47	-4.00	21.06

The modified wax composition, which presents a total wax value of 14.77%, is presented in Table 9.2.

Table 9.2: n-alkane modified composition

Component	wt %						
C5	0.2036	C16	0.5878	C27	0.0958	C38	0.0144
C6	0.7285	C17	0.5085	C28	0.0814	C39	0.0112
C7	1.2544	C18	0.4399	C29	0.0691	C40	0.0088
C8	1.4204	C19	0.3806	C30	0.0587	C41	0.0068
C9	1.3588	C20	0.3292	C31	0.0499	C42	0.0053
C10	1.2131	C21	0.2848	C32	0.0424	C43	0.0041
C11	1.2131	C22	0.2464	C33	0.0360	C44	0.0032
C12	1.0495	C23	0.1839	C34	0.0306	C45	0.0025
C13	0.9079	C24	0.1562	C35	0.0306	C46	0.0020
C14	0.7854	C25	0.1327	C36	0.0238	C47	0.0015
C15	0.6795	C26	0.1128	C37	0.0186		

A comparison of the original and modified wax compositions is presented in Fig.9.2. The modified composition presents slightly higher wax content for lower carbon numbers and smaller wax composition values for higher carbon numbers, as intended.

**Figure 9.2:** Original and modified paraffin compositions

Both compositions present an acceptable match considering the wax content, making it possible to use both wax compositions to describe the wax deposition process analyzed in the present work.

It is important to mention that only the n-alkane composition is modified, while the single carbon number composition of the oil (red line in Fig.9.1) remains the same for all characterizations.

After doing the oil characterization in Multiflash[®], based on the SCN composition and the n-alkanes compositions (original and modified), an equation of state (EoS) and wax model have to be selected to generate the information needed by OLGA[®]. The wax model used in this project, which is the only one available in Multiflash[®], is the Coutinho's model. When the wax model is selected, the Cubic Plus Association (CPA) EoS is automatically used by Multiflash[®] to perform flash calculations considering gas, oil and wax phases. Thus, the CPA-EoS is used in the present project.

If other EoS is required to describe the behavior of the fluid, a standalone file of flash calculations can be generated without including the wax fraction; this does not have a significant effect on the fluid properties [32].

Using the Multiflash[®] components option, the gas phase is directly characterized based on the information presented in Table 8.4. Liquid and gas characterizations are compared with values of physical properties calculated using the expressions reported by Rittirong[28] and Chi[15] (see Table 8.5) in order to validate the fluid characterization performed in Multiflash[®]. Table 9.3 shows the above mentioned comparison. It is important to mention that the properties of the oil are not affected by the characterization of the wax (original or modified); so, the oil properties presented in Table 9.3 are representative for both characterizations (original and modified).

Table 9.3: Validation of fluid characterization

Parameter	Reference	Value	Error (%)	Reference	Value	Error (%)
		5.00 °C			45.00 °C	
Oil properties						
Density	842.36	818.46	2.84	813.83	799.50	1.76
Thermal conductivity	0.20	0.15	24.68	0.18	0.14	17.66
Heat capacity	1.97	1.84	6.44	2.12	2.05	2.99
Viscosity	6.10	6.67	9.30	2.10	2.73	30.05
Gas properties						
Density	20.54	20.87	1.60	17.44	17.67	1.32
Thermal conductivity	0.03	0.03	3.49	0.4	0.4	2.27
Heat capacity	2.32	2.31	0.16	2.12	2.35	10.94
Viscosity	0.01	0.01	5.50	0.01	0.01	6.17

Units: density- kg/m^3 , thermal conductivity- $W/(mK)$, heat capacity- $kJ/(kgK)$, viscosity- cP

The gas characterization done in Multiflash[®] presents closer results regarding fluid properties than oil characterization. However, both are considered acceptable based on the premise that the fluid property expressions reported by Rittirong[28] and Chi[15] were calculated using a different EoS (SRK).

After the validation of the oil characterization the WAT is checked. Table 9.4 presents the WAT values obtained in Multiflash[®] and OLGA[®] for the oil characterizations done using the original wax composition and the modified one.

Table 9.4: WAT for characterized oils

Characterization	WAT (°C) - Multiflash [®]		WAT (°C) - OLGA [®]	WAT (°C) - DSC
	0.045 wt%	0.3 wt%	0.0 wt%	Experimental
Original	29.77	10.53	46.54	35.5
Modified	25.83	7.91	35.32	

The values of WAT estimated by Multiflash[®] differ considerably from the experimental value (35.5 °C); however, Multiflash[®] has an additional option for tuning the wax model, which produces results closer to the experimental WAT value. To use this option, the information provided by Rittirong[28] and Chi[15], regarding wax precipitation curve, could be used to tune the model. However, this tuning option is not applied in the present work due to higher discrepancies obtained between the estimated and the experimental WAT, since the first point of the wax precipitation curve (0.0 wt%) is moved at higher temperature values when the model is tuned in Multiflash[®]. In other words, when the Multiflash[®] tuning option is applied, the WAT reported by OLGA[®] is even higher, which is an undesired result.

The behavior of the wax precipitation curves for different characterizations can be clearly observed in Fig.9.3, where a comparison of experimental DSC data, Erickson's thermodynamic model prediction (used in Rittirong[28] and Chi[15] works) and Coutinho thermodynamic model predictions (available in Multiflash[®]) is presented.

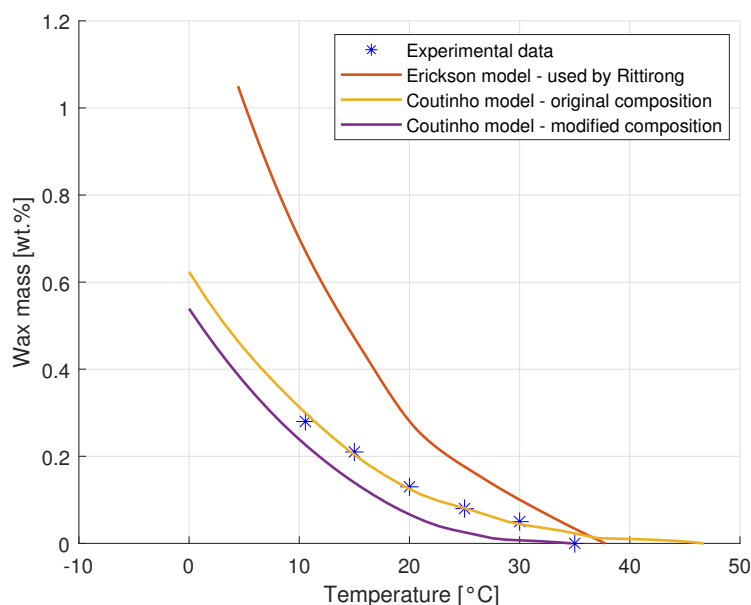


Figure 9.3: Precipitation curves comparison

Erickson's and Coutinho's models used for the precipitation curves presented in Fig.9.3 use the same experimental data, which corresponds to the data used by Rittirong[28] and Chi[15].

Considering the experimental data of Fig.9.3, Erickson's model (orange line) predicts

higher values for wax precipitation; on the other hand, Coutinho's model (yellow line) fits better to the wax experimental values. Such result was expected and agrees with the information presented in Fig.3.2. As can be seen in Fig.9.3, the prediction based on the wax original composition (yellow line) has a better match than the prediction made using the modified wax composition (violet line); however, the first point of the curve (0.0 wt% of wax) for the original wax composition appears at 46.54 °C while the first point of the modified composition appears at 35.32 °C. These two temperatures are the corresponding wax appearance temperatures, for original and modified wax composition that OLGA[®] takes to perform wax deposition calculations. The same two values of WAT are used also in the Matlab[®] runs for comparison of results.

After the oil and gas characterizations, the fluid blending process is done using the blend fluid option available in Multiflash[®]. The corresponding amounts of oil and gas are used according to the information presented in Table 8.7.

The last step in Multiflash[®] corresponds to the generation of PVT and WAX tables, which are used by OLGA[®] as simulation inputs. These tables are generated in the Import/Export option presented by Multiflash[®] for pressure and temperature ranges of 0.10 - 3.44 MPa and -10 - 80 °C, respectively.

The flow chart presented in Fig.9.4 shows the process followed in Multiflash[®] to characterize the fluid considering three phases (oil, gas and wax).

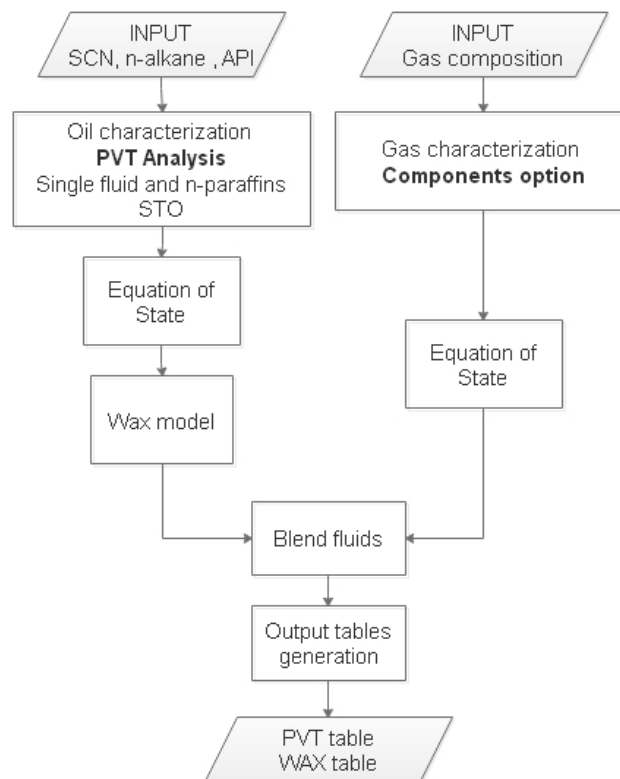


Figure 9.4: Precipitation curves comparison

A summary of the 16 study cases are presented in Table 9.5. The liquid and gas mass flows for each group of cases are based on the information presented in Table 8.7. Simi-

larly, E stands for the experimental data used in the present project and m for modified wax characterization.

Table 9.5: Study cases for analysis based on experimental data

Main cases		Study cases		
1E	1E-10d	1E-30d	1Em-10d	1Em-30d
2E	2E-10d	2E-30d	2Em-10d	2Em-30d
3E	3E-10d	3E-30d	3Em-10d	3Em-30d
4E	4E-10d	4E-30d	4Em-10d	4Em-30d

As an example, considering the first main case 1E, the four study cases related to this main case are:

- 1E-10d, where the fluid characterization is done based on the information presented in Tables 8.1,8.2,8.3 and 8.4, which corresponds to the original information provided by Rittirong and Chi [28, 15]. This study case is analyzed for a deposition time of 10 days.
- 1E-30d, this study case uses the same fluid characterization described for the case 1E-10d. The present case differs in the deposition time considered for analysis which is equal to 30 days.
- 1Em-10d, where the fluid characterization is done based on the information presented in Tables 8.1,8.2 and 8.4, which corresponds to the original information provided by Rittirong and Chi [28, 15]; however, the n-alkane composition used in this study case is a modified version that is presented in Table 9.2. This study case is analyzed for a deposition time of 10 days.
- 1Em-30d, this study case uses the same fluid characterization described for the case 1Em-10d. The present case differs in the deposition time considered for analysis which is equal to 30 days.

It is important to note that these 16 study cases are analyzed in OLGA[®] and Matlab[®], and their comparative results will be presented in corresponding section (Chapter 11).

9.1.2 Pipeline characteristics

In this section all characteristics used in OLGA[®] regarding pipeline are presented.

Properties of the pipeline material corresponds to steel with a heat capacity of $500 J/(kg^{\circ}C)$, heat conductivity of $45 W/(mK)$ and density of $7850 kg/m^3$. These properties are included in the software library regarding structural-material properties. In the same library, the pipeline thickness is defined according to the information presented in Table 8.6.

When the pipeline is created in the software interface, pipe length and roughness are established based on the information provided in Table 8.6. Finally, the number of sections in which the pipeline is split to increase the accuracy of the calculation is set. In the present project, 300 sections are used in the OLGA[®] simulation, according to the independence analysis presented in section 9.2.1.

9.1.3 Process conditions

This section includes the conditions considered in the simulations performed in OLGA[®] using experimental data.

In addition to the pipeline components, an inlet source and outlet nodes are created in the software interface. In these components the inlet temperature, fluid mass flow and outlet pressure are set according to the information presented in Tables 8.6 and 8.7.

When wax deposition process is analyzed in OLGA[®], heat transfer calculations cannot be performed based on a given overall heat transfer coefficient - OHTC (U). Instead of this, the inner wall and ambient heat transfer convective coefficients (h_{inwall} , h_{amb}) can be provided to the software in order to run wax deposition simulations. Thus, trying to maintain the same conditions between OLGA[®] and Matlab[®] simulations, and considering that the code developed in Matlab[®] uses a constant value of OHTC equal to $20 W/(m^2K)$, a trial and error analysis is done varying the h_{amb} to find an OHTC closer to $20 W/(m^2K)$, as is seen in Table 9.6. In all scenarios, the inner convective coefficient h_{inwall} is maintained constant and equal to $20 W/(m^2K)$.

Table 9.6: Heat transfer coefficients used in OLGA[®] simulation

Main case	h_{amb} $W/(m^2K)$	U $W/(m^2K)$
1E	24.5	18.6 - 20.8
2E	22.0	19.1 - 20.8
3E	21.5	19.8 - 20.2
4E	21.9	19.9 - 20.1

The range of OHTC values presented in Table 9.6 varies around the constant OHTC value used in Matlab[®] ($20 W/(m^2K)$); this approach provides a similar heat transfer scenario for wax deposition evaluation.

The values presented in Table 9.6 apply for the corresponding study cases (4 for each main case).

9.2 Wax deposition simulation setup

The setup of the simulation for wax deposition analyses is shown in the present section considering simulation based on experimental data.

The wax deposition option must be included in the simulation to run this kind of analyses. Such option is defined under the option FA-models (flow assurance models), which are available in OLGA[®] [32].

After the activation of the wax deposition module in the simulation environment, the Matzain model available in OLGA[®] is selected. The empirical constants C_2 and C_3 (Eq.6.4), which are related to the wax removal due to shear stripping, are defined according to the values provided by Matzain which are 0.055 and 1.4, respectively [26]. The empirical constant $C_1 = 15$, which attempts to correct the offset in wax deposition prediction considering that flow turbulence enhances the diffusion process via turbulent eddies

effect, is included directly inside the software code, and it cannot be modified; however, OLGA[®] presents a diffusion coefficient multiplier which modifies directly the values of the diffusion coefficient calculated by the wax deposition model [33]. According to Leporini et al. [11] the diffusion coefficient multiplier is the most important tuning value for wax deposition evaluations when Matzain model is used in OLGA[®]. All the simulation cases of the present project use a diffusion coefficient multiplier equal to 1.

9.2.1 Discretization independence analysis

The independence analyses are performed in order to define the best number of sections in which the pipeline should be divided in order to obtain a balance between accuracy and computation cost.

For the independence analysis performed based on experimental data, pressure drop and outlet temperature are analyzed considering different number of pipeline sections. Figure 9.5 presents the results for the independence analysis made for the study case 3E-10d. It is important to note that all cases present the same trend shown in the following figure.

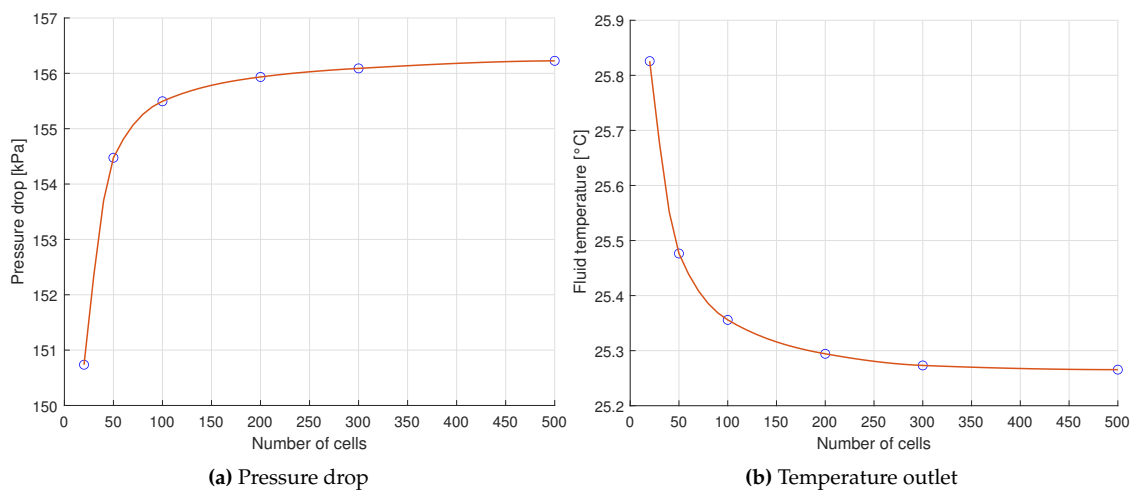


Figure 9.5: Discretization independence analysis OLGA

As expected, the pressure drop increases when the number of sections is increased, but an asymptotic trend is observed at a value around 200 sections. In addition, the fluid temperature outlet decreases when the number of pipeline sections is increased, showing almost constant temperature values around 300 sections. Thus, a number of 300 sections is considered adequate for having a balance between accuracy and computation cost.

The variations of pressure drop and temperature presented in Fig.9.5 are small and can be considered as a non-significant; however, this kind of study should be visualized as a trend evaluation analysis in order to select an acceptable simulation balance.

9.2.2 Stability analysis

Regarding the time step for wax deposition calculations, OLGA[®] uses a time step of 3600 s approximately, regardless the input parameters provided. This is not a constant time step, it varies around this value giving the idea that the software calculates the time step based on other unknown parameters.

10 Wax deposition using Matlab[®]

This section presents the methodology used in the entry data treatment and modeling setup for wax deposition analysis using Matlab[®]. It is important to note that this is a very simplified modeling for wax deposition phenomenon; thus, many assumptions are made during the model development. This methodology applies for the experimental data considering horizontal pipelines, and it is based on the Matzain model for wax deposition. The appendix of this document shows the code developed for the current project.

10.1 Entry data treatment

The entry data treatment shows some simplifications done for different parameters required as input data in the code developed in Matlab[®] in order to perform a simple but representative modeling of wax deposition phenomenon. Average values for fluids properties and other process characteristics are included in this section considering a fluid temperature of 32.5 °C. This temperature corresponds to the average value between 60 °C and 5 °C which are the inlet and expected outlet fluid temperatures, respectively, considering the entire pipe length.

Oil and gas properties are estimated using the equations presented in Table 8.5 considering the average fluid temperature of 32.5 °C. Additionally, Table 10.1 presents the average properties used in the Matlab[®] code.

Table 10.1: Fluid properties used in Matlab[®] [15, 28]

Parameter	Symbol	Units	Value
Oil average properties			
Density	ρ_o	kg/m^3	822.74
Thermal conductivity	k_o	$W/(mK)$	0.18
Heat capacity	Cp_o	$J/(kgK)$	2074.21
Viscosity	μ_o	cP	3.00
Interfacial tension	σ	mN/m	16.25
Gas average properties			
Density	ρ_g	kg/m^3	18.41
Thermal conductivity	k_g	$W/(mK)$	0.04
Heat capacity	Cp_g	$J/(kgK)$	2357.30
Viscosity	μ_g	cP	0.011

In addition, typical values for wax density and molecular weight, presented in Table 10.2, are used as part of the Matlab[®] entry data needed for wax deposition analysis.

Table 10.2: Wax properties used in Matlab[®] [34, 35, 36]

Parameter	Symbol	Units	Value
Density	ρ_w	kg/m^3	900
Molecular weight	MW_w	g/mol	475

The code developed in Matlab[®] uses a constant overall heat transfer coefficient (OHTC) which is equal to $20 W/(m^2K)$. This value is taken as an average of the typical OHTC values reported by Bai [4] and Gudmundsson [17] for bare steel pipes, which oscillate from 15 to $25 W/(m^2K)$.

The process conditions and pipeline characteristics used in the Matlab[®] code correspond to the values presented in Table 8.6.

In addition, the Matlab[®] code is run for the 16 study cases presented and explained in Table 9.5. As input data, this code requires the wax appearance temperature (WAT) of each study case; thus, $46.5\text{ }^\circ\text{C}$ is used as WAT for the cases that use original n-alkane composition, and $35.5\text{ }^\circ\text{C}$ as the WAT for modified composition cases.

Finally, as entry data for Matzain wax deposition model the constants $C_1 = 15.0$, $C_2 = 0.055$ and $C_3 = 1.4$ are used as stated in the model description (section 6).

10.2 Modeling setup

Using the input data the wax deposition phenomenon is modeled through the code developed in Matlab[®]. The following methodology is applied to accomplish the wax deposition prediction.

10.2.1 Heat transfer calculations

Considering the heat transfer calculation the bulk and inner wall temperatures are estimated. These two temperatures are calculated in a steady-state scenario, and are useful for the wax deposition analysis [17].

The bulk temperature is calculated through Eq.10.1.

$$T_2 = T_{amb} + (T_1 - T_{amb}) \exp\left[\frac{-U\pi d}{\dot{m}C_p}\right] L \quad (10.1)$$

Where T_1 , T_2 and T_{amb} are the pipe section inlet, outlet and ambient temperatures (K) respectively, U is the overall heat transfer coefficient - OHTC ($W/(m^2K)$), d is the pipe inner diameter (m), \dot{m} is the total mass flow rate (kg/s), C_p is the fluid heat capacity ($kJ/(kgK)$) and L is the pipe section length (m).

The internal convection coefficient is estimated from the Nusselt dimensionless number which is found applying the Sieder and Tate correlation (Eq.10.2) for laminar flow, and Dittus-Boelter (Eq.10.3), Sieder and Tate (Eq.10.4) and Whitaker (Eq.10.5) correlations for turbulent flow. Each correlation applies to different ranges of Reynolds and Prandtl numbers as indicated in the corresponding equations. In these correlations, the effect of the viscosity ratio is neglected because the Matlab[®] code does not consider the viscosity as a

function of temperature. Then, the general heat flux equation or Newton's Law of Cooling (Eq.10.6) is used to determine the inner wall temperature [17, 37].

It is important to mention that in the calculation approach used to determine the inner wall temperature, the fluid is considered as a homogeneous flow, not as multiphase fluid flow. This assumption has a direct impact on the Reynolds number calculation.

$$Nu = 1.86(RePr(d/L))^{1/3} \quad (10.2)$$

$$\text{For } 13 \leq Re \leq 2030 \quad 0.48 \leq Re \leq 16700$$

$$Nu = 0.023Re^{0.8}Pr^{0.3} \quad (10.3)$$

$$\text{For } Re \geq 10000 \quad 0.7 \leq Re \leq 160$$

$$Nu = 0.027Re^{4/5}Pr^{1/3} \quad (10.4)$$

$$\text{For } Re \geq 10000 \quad 0.7 \leq Re \leq 16700$$

$$Nu = 0.015Re^{0.83}Pr^{0.42} \quad (10.5)$$

$$\text{For } 2300 \leq Re \leq 100000 \quad 0.48 \leq Re \leq 592$$

Where Nu , Re and Pr are the Nusselt, Reynolds and Prandlt dimensionless numbers respectively, d is the internal diameter (m) and L is the pipe length (m).

$$\frac{q}{A} = \frac{(T_i - T_o)}{R} \quad (10.6)$$

Where q/A is the heat flux (W/m^2), T_i and T_o are the inner and outer temperatures, respectively (K) and R is the heat transfer resistance (m^2K/W).

10.2.2 Hydrodynamic calculations

The hydrodynamic calculations are constituted by two main parts: pressure drop calculations and multiphase flow regime determination, both considering no-changes in pipe elevation and diameter.

Pressure drop

The pressure drop estimations are performed based on one-phase pressure drop analysis considering all fluid as liquid. Moreover, Gudmundsson states that the multiphase pressure drop is typically ten times greater than single-phase pressure drop [17]; thus, the previous results are multiplied by ten in order to obtain a more realistic value of multiphase pressure drop in pipelines.

For flow in horizontal pipelines without changes in inner diameter, the pressure drop only corresponds to losses due to friction calculated through Darcy-Weisbach Equation, where the friction factor determination plays a main role.

The friction factor for laminar flow ($Re < 2100$) is calculated by Eq.10.7. When the flow is turbulent ($Re > 4000$) the friction factor is computed applying Haaland Equation for liquids (Eq.10.8). For flows that obey to transition regime ($2100 < Re < 4000$) an average of laminar and turbulent friction factors is used for pressure drop calculation.

$$f = \frac{64}{Re} \quad (10.7)$$

Where f is the Darcy's friction factor

$$\sqrt{\frac{1}{f}} = -1.8 \log \left[\frac{6.9}{Re} + \left(\frac{\epsilon}{3.75d} \right)^{1.11} \right] \quad (10.8)$$

Where ϵ is the pipeline roughness (m) and d is the pipe inner diameter (m).

Flow pattern map

The flow regime is determined through Mandhane et al. two-phase regime map (Fig. 5.2), which was published in the work: *A flow pattern map for gas-liquid flow in horizontal pipes* [25].

Mandhane et al. two-phase regime map uses liquid and gas superficial velocities (Eq.5.1) to determine the flow pattern.

According to Mandhane et al. their map presents a small effect of the physical fluid properties. So, it can be used for several fluids without any map correction [25].

In the present project the Mandhane et al. two-phase regime map is slightly modified in order to predict flow patterns useful for wax deposition Matzain model [26]. The coded flow map predicts stratified & wavy and bubble & slug as two flow regimes instead of four separated flow regimes, as is presented in the Mandhane et al. two-phase regime map. The reason for this modification is based on the fact that Matzain model uses Eq.6.7 to estimate the Reynolds number to account the limiting deposition effect due to shear stripping for stratified & wavy flow and Eq.6.8 for bubble & slug flow, which makes unnecessary the identification of four different flow patterns.

Table 10.3 shows the transition boundaries used in the Matlab[®] code to determine the different flow regimes.

Among other variables, the multiphase flow regime and liquid holdup (E) are needed in the determination of the Matzain constant (π_2) regarding wax removal due to shear stripping. The liquid holdup is estimated through Eq.10.9 [38].

$$E = \frac{1}{1 + \left(\frac{u_M}{8.66} \right)^{1.39}} \quad (10.9)$$

Where u_M is the mixture velocity and is equal to the sum of the gas and liquid superficial velocities.

Table 10.3: Coordinates for transition boundaries

Boundary	u_{sg} (ft/s)	u_{sl} (ft/s)
	0.1	0.5
Stratified & Wavy to Slug & Bubble	5.0	0.5
	7.5	0.3
	40.0	0.3
Stratified & Wavy to Annular	40.0	0.3
	70.0	0.01
Slug & Bubble to Annular	40.0	0.3
	230	14
Slug & Bubble to Dispersed	0.1	14
	230	14
Dispersed to Annular	230	14
	269	30

10.2.3 Thermodynamic calculations

The thermodynamic analysis developed in the Matlab[®] code has a simple approach which only considers the wax precipitation curve. In other words, the equations that describe the behavior of the precipitation curves presented in Figure 9.3, for original and modified wax compositions, are used to estimate the wax weight fraction as a function of temperature.

The behavior observed in the precipitation curves is described under the cubic equations (Eqs.10.10 and 10.11) for original and modified wax composition, respectively. As explained in the Entry data treatment (section 10.1), the WAT for original and modified n-alkanes composition are 46.5 and 35.5 °C, respectively.

$$w_{pf} = -6.618E - 8 * T^3 + 6.290E - 5 * T^2 - 1.994E - 2 * T + 2.109 \quad (10.10)$$

$$w_{pf} = -6.92E - 8 * T^3 + 6.589E - 5 * T^2 - 2.090E - 2 * T + 2.208 \quad (10.11)$$

Where w_{pf} is the wax precipitated fraction and T is the temperature, expressed in K .

The w_{pf} is calculated for two temperatures (bulk and wall ones). Finally, each w_{pf} is subtracted from the total content of wax, which is equal to 4.3% (Table 8.1), resulting in the fraction of wax that is still available and dissolved in the hydrocarbon fluid.

The derivative of Eqs.10.10 and 10.11 are used in the wax deposition calculation presented in the following section.

10.2.4 Wax deposition calculations

The wax deposition calculations are performed applying the Matzain model described in section 6. All the equations presented in the mentioned section (Eqs from 6.1 to 6.10) are used to perform wax deposition estimations considering deposit through length and deposition evolution over time.

It is important to mention that the wax deposition modeling using Matlab[®] consists in an iterative computation process which includes heat transfer, hydrodynamic and wax deposition calculations considering that each time step means an increment in the wax deposit layer and consequently a variation in the heat transfer, hydrodynamic and wax deposition phenomena mainly due to a continuous reduction in the inner diameter.

10.2.5 Discretization independence analysis

The pipeline is discretized in a certain number of sections in order to obtain accurate results when the different modules are run in the code.

The effect of different number of pipe sections on pressure drop and temperature outlet is evaluated in this independence analysis, as is shown in Fig.10.1.

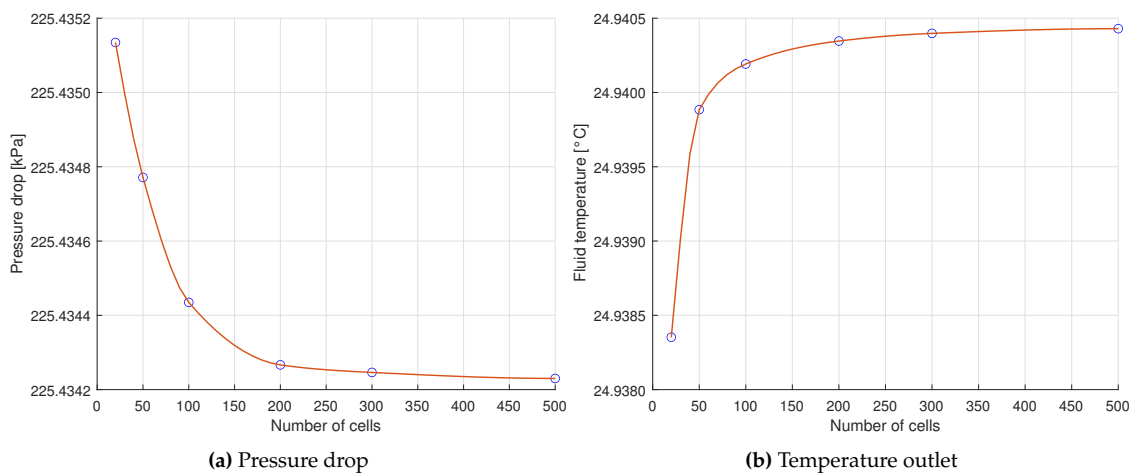


Figure 10.1: Discretization independence analysis Matlab

Even though the variations of pressure drop and temperature values for different number of cells are almost negligible, a stable behavior is observed when 300 cells are considered for running the Matlab[®] code. This number of cells presents an acceptable balance between pressure drop behavior and computational cost.

The small variations in pressure drop and temperature could be attributed to the assumption of constant fluid properties used in the code developed in Matlab[®].

10.2.6 Stability analysis

A stability analysis regarding the size of the time step for wax deposition calculations is presented in this section.

The effect of different time steps on the deposit thickness is evaluated, as is shown in Fig.10.2. The study case 1E-10d is considered in the present analysis.

Small variations in wax thickness is observed for different time steps; however, a stable trend is shown for time steps lower than 1000 s. Thus, in order to maintain a good balance between simulation accuracy and computational cost a time step of 1000 s is considered in all wax deposition simulations performed in Matlab[®].

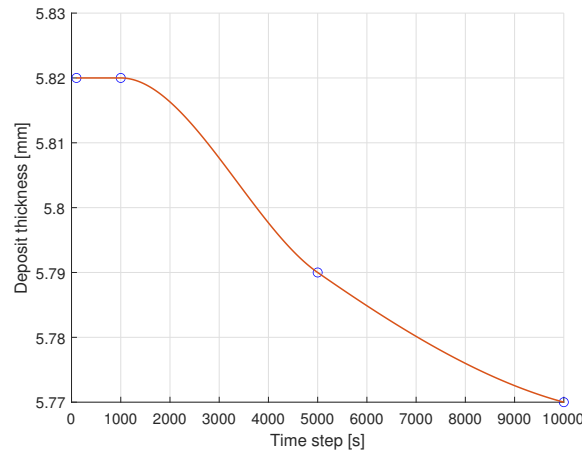


Figure 10.2: Time step stability analysis

10.2.7 Modeling flow chart

The Matlab[®] routine used for modeling the wax deposition process is summarized in Fig. 10.3 where a general overview of all modules coded in Matlab[®] is presented.

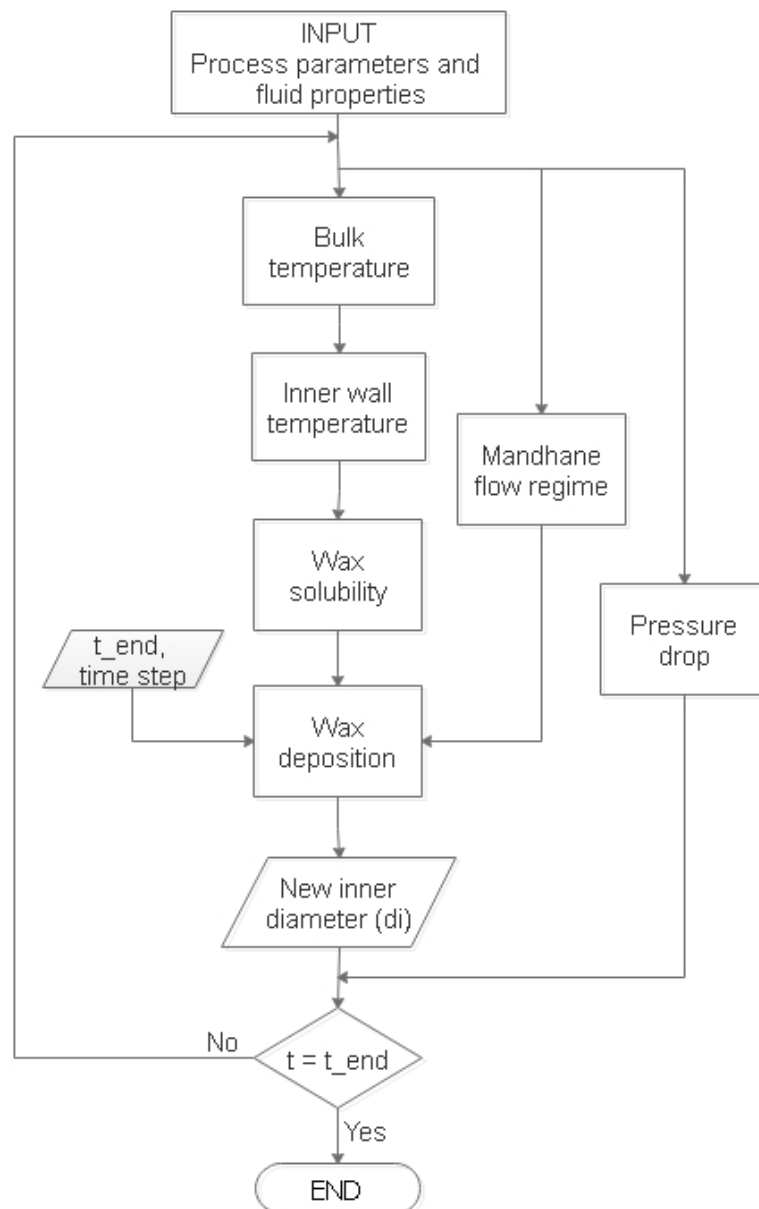


Figure 10.3: Wax deposition through molecular diffusion.

11 Results

This section presents the results obtained based on the experimental data using OLGA[®] and Matlab[®] code.

The 16 study cases presented in Table 9.5 were run in OLGA[®] and Matlab[®]; however, some results can be considered as representative of the four study cases corresponding to a main case. For instance, results regarding bulk temperature calculation for cases 1E-10d, 1E-30d, 1Em-10d and 1Em-30d are well represented by the results of only one of this cases, which is presented as the main case 1E.

These representative results are used in the interpretation of data resulting from the analysis of the following variables:

- Bulk and wall temperatures
- Pressure drop
- Superficial velocities
- Flow pattern prediction
- Wax precipitation

On the other hand, the wax deposition analyses show the results of the 16 cases run in OLGA[®] and Matlab[®].

11.1 Heat transfer and fluid mechanics along the pipeline

Results regarding heat transfer and fluid mechanics analysis are presented in this section. As previously stated, this section presents representative results for each main case namely 1E, 2E, 3E and 4E. This means that the differences in fluid characterization (original and modified wax composition) as well as wax deposition times (10 and 30 days) do not present a significant effect over the variables presented in this section.

11.1.1 Bulk and wall temperatures

This section presents the results regarding bulk and wall temperature profiles along the pipeline length. The results for main cases 1E and 2E as well as for main cases 3E and 4E are shown in Figs.11.1 and 11.2, respectively.

Bulk temperature profiles for main cases 1E and 2E, calculated using OLGA[®] and Matlab[®] code, present similar behavior along the pipeline with close temperature values resulting of both codes. The system fluid-pipeline reaches the ambient temperature at 8 and 10 km for main cases 1E and 2E, respectively. These distances are found similar in the

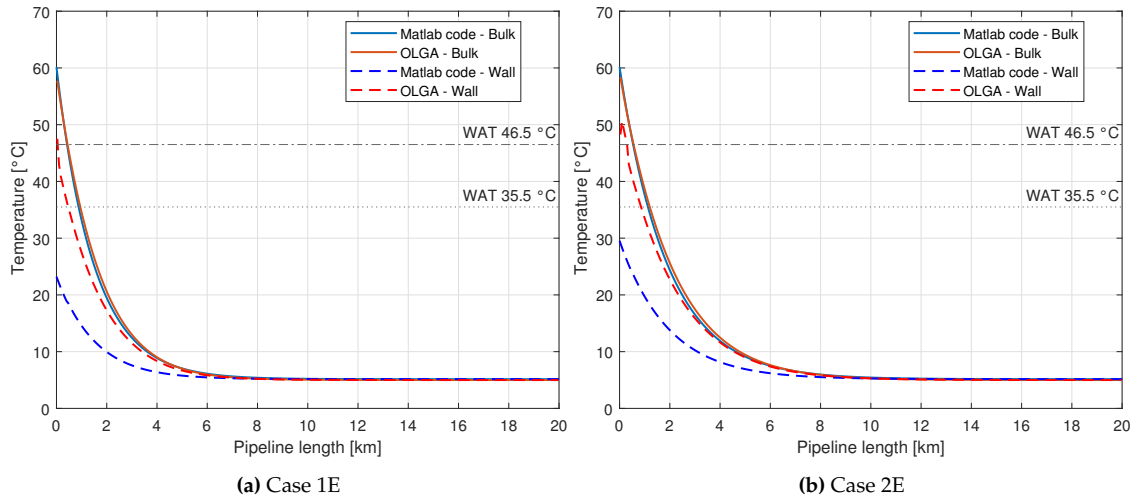


Figure 11.1: Bulk and wall temperature profile - Cases 1&2 E/Em

results obtained by OLGA[®] and Matlab[®] simulations. These results let infer that the model used for bulk temperature prediction in Matlab[®] is appropriate and works well even considering a homogeneous fluid flow.

In main cases 1E and 2E, the wall temperature profiles obtained through OLGA[®] and Matlab[®] show a significant difference which can be attributed to the different heat transfer calculation approach used in both codes. OLGA[®] considers a multiphase heat transfer approach together with fluid properties variation with temperature, while the code developed in Matlab[®] uses a homogeneous fluid approach in addition to constant fluid properties. Thus, the calculation of the film heat transfer resistance (R - Eq.10.6) is affected by Reynolds and Prandtl number determinations.

Moreover, the fluid velocity used in the calculation of Reynolds number (Eqs. from 10.2 to 10.5) has an important effect on the wall temperature determination. In fact, Lindeloff mentions about some difficulties regarding this calculation algorithm due to the high sensitivity related to the determination of the film heat transfer coefficient [39].

Table 11.1 shows the position in the pipeline at which the WAT is reached considering the bulk temperature.

Table 11.1: Pipeline length where WAT is reached - 1&2 E Bulk temperature

Main cases	WAT = 46.5 °C		WAT = 35.5 °C	
	OLGA [®]	Matlab [®]	OLGA [®]	Matlab [®]
1E	0.46	0.50	0.93	0.96
2E	0.60	0.56	1.13	1.20

All values in this table are expressed in *km*

As was observed in Fig.11.1, the bulk temperature results present similar values considering the OLGA[®] and Matlab[®] simulations. These results agree with the positions at which the bulk temperatures of the fluids reach the corresponding WAT. Considering the main case 1E, the WAT of 46.5 °C is reached around 0.48 km; on the other hand, at around 0.95 km the WAT of 35.5 °C is attained. This means the pipe position at which wax formation and deposition begin for cases 1E (original wax characterization) and 1Em (modified

wax characterization) is located at 0.48 and 0.95 km, respectively. Doing a similar analysis for cases 2E (original wax characterization) and 2Em (modified wax characterization) the starting points for wax formation and deposition are located at 0.58 and 1.16 km, respectively. Generally speaking, the wax appearance of main case 2E is slightly further in pipe length in comparison with main case 1E due to the higher mass flow of the case 2E.

Table 11.2 presents the position in the pipeline at which the WAT is reached considering the wall temperature.

Table 11.2: Pipeline length where WAT is reached - 1&2 E Wall temperature

Main cases	WAT = 46.5 °C		WAT = 35.5 °C	
	OLGA [®]	Matlab [®]	OLGA [®]	Matlab [®]
1E	0.10	N/A	0.50	N/A
2E	0.30	N/A	0.90	N/A

All values in this table are expressed in *km*

The high difference regarding wall temperature calculations observed in Fig.11.1 considering OLGA[®] and Matlab[®] simulations is also appreciable when the starting point for wax formation and deposition using wall temperature is performed. In main cases 1E and 2E, Matlab[®] results cannot be estimated because the initial wall temperatures calculated using this code present lower values than the corresponding WATs; in other words, based on the wall temperature, the wax formation and deposition process should begin before the fluid entering into the pipeline.

Considering the results obtained through OLGA[®], the pipe position at which wax formation and deposition begin for cases 1E (original wax characterization-WAT 46.5 °C) and 1Em (modified wax characterization-WAT 35.5 °C) are located at 0.10 and 0.50 km, respectively. Doing a similar analysis, for cases 2E (original wax characterization) and 2Em (modified wax characterization) the starting points for wax formation and deposition are located at 0.30 and 0.90 km, respectively.

Figure 11.2 shows the results of bulk and wall temperatures related to main cases 3E and 4E calculated using OLGA[®] and Matlab[®] code. Both temperature profiles present similar behavior along the pipeline with close temperature values resulting of both codes. In the main cases 3E and 4E, the system fluid-pipeline does not reach the ambient temperature since the mass flows considered are higher than the flows for main cases 1E and 2E.

In main cases 3E and 4E, the wall temperature profiles obtained through OLGA[®] and Matlab[®] show a similar behavior in contrast to the results obtained for main cases 1E and 2E. The closer resultant values can be explained considering a higher accuracy of the Matlab[®] wall temperature prediction. The liquid mass fractions presented by these two cases (3E and 4E - Table 8.7) are higher than 0.90; thus, fluid velocity presented by the multiphase flow in OLGA[®] has a better similitude with the one-phase and homogeneous fluid flow approach used in the Matlab[®] code. At the end, the different heat transfer approaches used in both codes do not suffer significant differences when wall temperature results are estimated.

Table 11.3 shows the position in the pipeline at which the WAT is reached considering the bulk temperature.

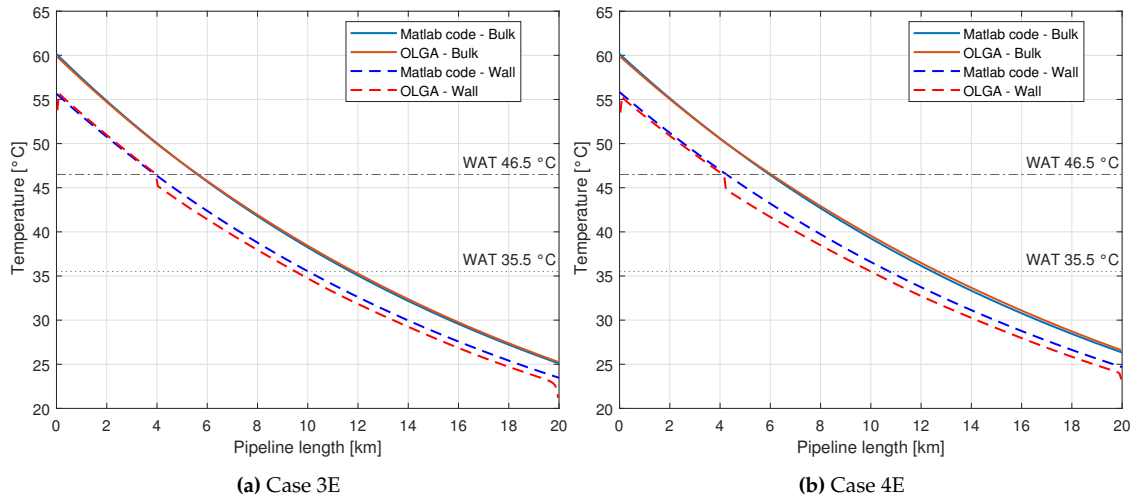


Figure 11.2: Bulk and wall temperature profile - Cases 3&4 E/Em

Table 11.3: Pipeline length where WAT is reached - 3&4 E Bulk temperature

Main cases	WAT = 46.5 °C		WAT = 35.5 °C	
	OLGA [®]	Matlab [®]	OLGA [®]	Matlab [®]
3E	5.60	5.70	11.73	11.90
4E	6.00	6.10	12.46	12.70

All values in this table are expressed in *km*

As was observed in Fig.11.2, the bulk temperature results present similar values considering the OLGA[®] and Matlab[®] simulations. This agrees with the positions at which the bulk temperatures of the fluids reach the corresponding WAT. Considering the main case 3E, the WAT of 46.5 °C is reached around 5.65 km; on the other hand, at around 11.81 km the WAT of 35.5 °C is reached. This means the pipe position at which wax formation and deposition begin for cases 3E (original wax characterization) and 3Em (modified wax characterization) are located at 5.65 and 11.81 km, respectively. Doing a similar analysis, for cases 4E (original wax characterization) and 4Em (modified wax characterization) the starting points for wax formation and deposition are located at 6.05 and 12.58 km, respectively. In general, the wax appearance of main case 4E is slightly further in pipe length in comparison with main case 3E due to the higher mass flow of the case 4E.

Table 11.4 presents the position in the pipeline where the WAT is reached considering the wall temperature.

Table 11.4: Pipeline length where WAT is reached - 3&4 E Wall temperature

Main cases	WAT = 46.5 °C		WAT = 35.5 °C	
	OLGA [®]	Matlab [®]	OLGA [®]	Matlab [®]
3E	3.93	3.96	10.06	9.59
4E	4.20	4.16	10.80	10.03

All values in this table are expressed in *km*

According to the information presented in Table 11.4 the positions at which the wall temperatures of the fluids reach the corresponding WAT for main cases 3E and 4E are similar

for the simulations performed in OLGA[®] and Matlab[®]. The pipe position at which wax formation and deposition begin for cases 3E (original wax characterization-WAT 46.5 °C) and 3Em (modified wax characterization-WAT 35.5 °C) are located at 3.95 and 9.82 km, respectively. Doing a similar analysis, for cases 4E (original wax characterization) and 4Em (modified wax characterization) the starting points for wax formation and deposition are located at 4.18 and 10.42 km, respectively.

The points 3.95 and 4.18 km for cases 3E and 4E respectively can be observed as small changes in the trends followed by the wall temperatures estimated through OLGA[®] simulations (Fig.11.2).

11.1.2 Pressure drop profile

This section presents the results regarding pressure drop along the pipeline. The results for main cases 1E and 2E as well as for main cases 3E and 4E are shown in Figs.11.3 and 11.4, respectively.

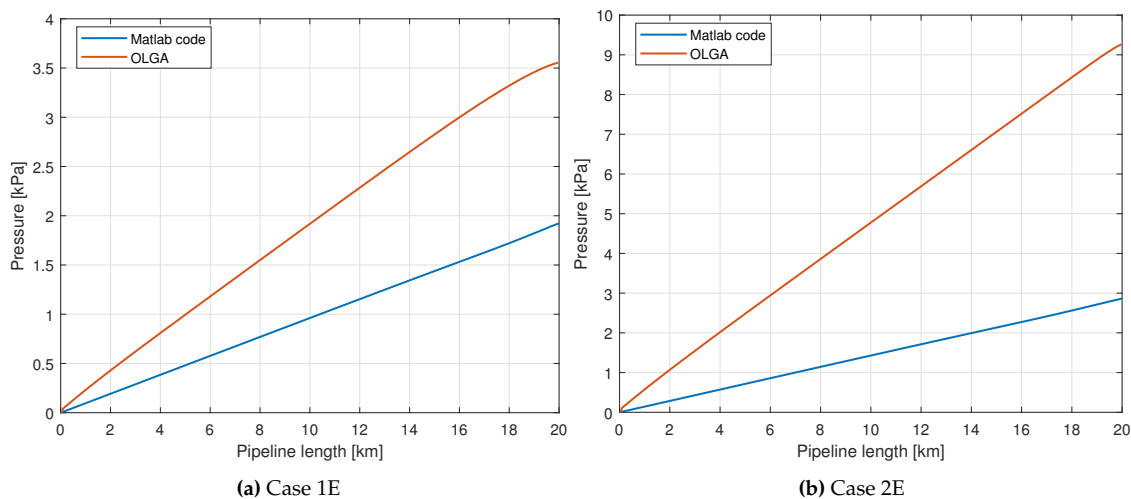


Figure 11.3: Pressure drop profile - Cases 1&2 E/Em

Pressure drop profiles for main cases 1E and 2E, calculated using OLGA[®] and Matlab[®] code, present similar behavior along the pipeline with close pressure drop values resulting of both codes. The total pressure drop observed for main case 1E is around 3.5 and 2.0 kPa using OLGA[®] and Matlab[®] simulations, respectively. Additionally, the total pressure drop observed for main case 2E is around 9.0 and 3.0 kPa using OLGA[®] and Matlab[®] simulations, respectively.

Generally speaking, the pressure drop calculation based on the criterion presented by Gudmundsson [17], which states that the multiphase pressure drop is ten times bigger than the liquid pressure drop, produces results with high similarities considering the main cases 1E and 2E.

The pressure drop predictions for main cases 3E and 4E are presented in Fig.11.4. Likewise, the pressure drop profiles for main cases 3E and 4E, calculated using OLGA[®] and Matlab[®] code, present similar behavior along the pipeline with close pressure drop values resulting of both codes. The total pressure drop observed for main case 3E is around 150 and 210 kPa using OLGA[®] and Matlab[®] simulations, respectively. Additionally, the total pressure drop observed for main case 4E is around 350 and 240 kPa using OLGA[®] and Matlab[®] simulations, respectively.

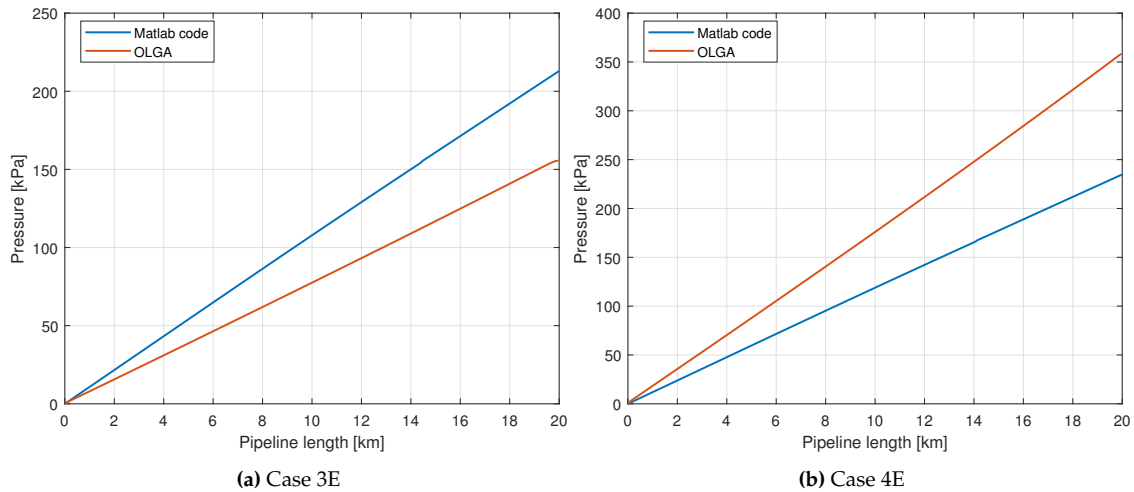


Figure 11.4: Pressure drop profile - Cases 3&4 E/Em

For case 3E, contrary to the behavior observed in the rest of the main cases (1E, 2E and 4E), calculations with Matlab[®] present a higher pressure drop than the one obtained with OLGA[®]. This behavior might be related to the pressure drop observed at higher liquid fractions (98%) for multiphase flow, which is slightly smaller than the criterion of Gudmundsson. In other words, for main case 3E, the multiphase flow pressure drop is seven times bigger than the one-phase pressure drop (considering all the fluid amount as liquid.) Nevertheless, Gudmundsson criterion seems acceptable for all main cases.

11.1.3 Superficial velocities

This section presents the results regarding superficial velocities profiles. The results for main cases 1E and 2E as well as for main cases 3E and 4E are shown in Figs.11.5 and 11.6, respectively.

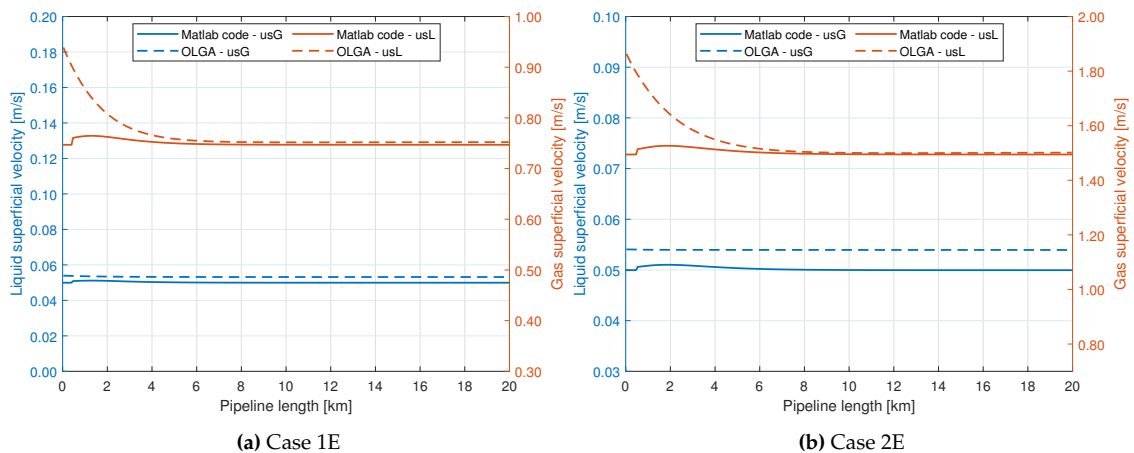


Figure 11.5: Superficial velocities - Cases 1&2 E/Em

Superficial velocities for main cases 1E and 2E, calculated using OLGA[®] and Matlab[®] code, present similar behaviors along the pipeline with close superficial velocity values resulting of both codes. The average fluid velocity for main case 1E is around 0.75 m/s for the gas phase and 0.05 m/s for the liquid phase. Considering the main case 2E, the average fluid velocities are around 1.50 m/s for the gas phase and 0.05 m/s for the liquid phase.

The divergence presented in the first section of the pipeline for gas superficial velocities between the results from OLGA[®] and Matlab[®] can be attributed to the significant change of bulk temperature observed in such first sections, affecting the density of the gas phase, which is correlated to the gas superficial velocity.

The predictions for superficial velocities for main cases 3E and 4E are presented in Fig.11.6.

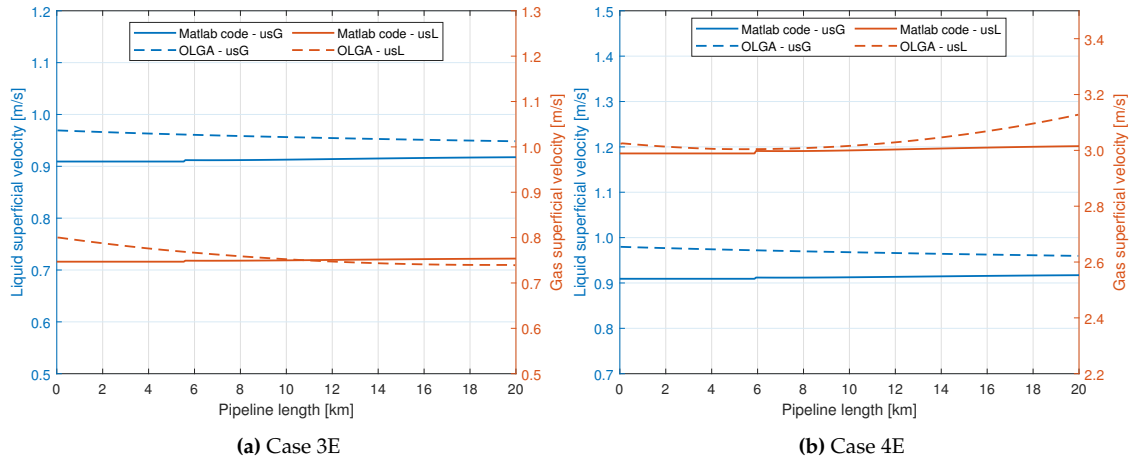


Figure 11.6: Superficial velocities - Cases 3&4 E/Em

Analogous to main cases 1E and 2E, superficial velocities for main cases 3E and 4E, calculated using OLGA[®] and Matlab[®] code, present similar behaviors along the pipeline with close superficial velocity values resulting of both codes. The average fluid velocity for main case 3E is around 0.75 m/s for the gas phase and 0.95 m/s for the liquid phase. Considering the main case 4E, the average fluid velocities are around 3.00 m/s for the gas phase and 0.95 m/s for the liquid phase.

In general, the observed differences in superficial velocities might be a consequence of different physical properties of the fluids as a result of the characterization approach used in OLGA[®] and the constant fluid properties consideration applied in Matlab[®].

11.1.4 Flow pattern prediction

This section presents the results regarding multiphase flow pattern predictions. Table 11.5 shows the results obtained through OLGA[®]. These agree with the flow pattern presented in the works done by Chi and Rittirong [15, 28].

Table 11.5: Flow pattern predictions

Case	Flow pattern
1E & 1Em	Stratified
2E & 2Em	Stratified
3E & 3Em	Slug
4E & 4Em	Slug

Main cases 1E and 2E present a stratified flow pattern while main cases 3E and 4E are defined as slug flows, according to the flow prediction made by OLGA[®].

The flow pattern predictions performed by the Matlab[®] code, for main cases 1E and 2E as well as for main cases 3E and 4E are shown in Figs.11.7 and 11.8, respectively.

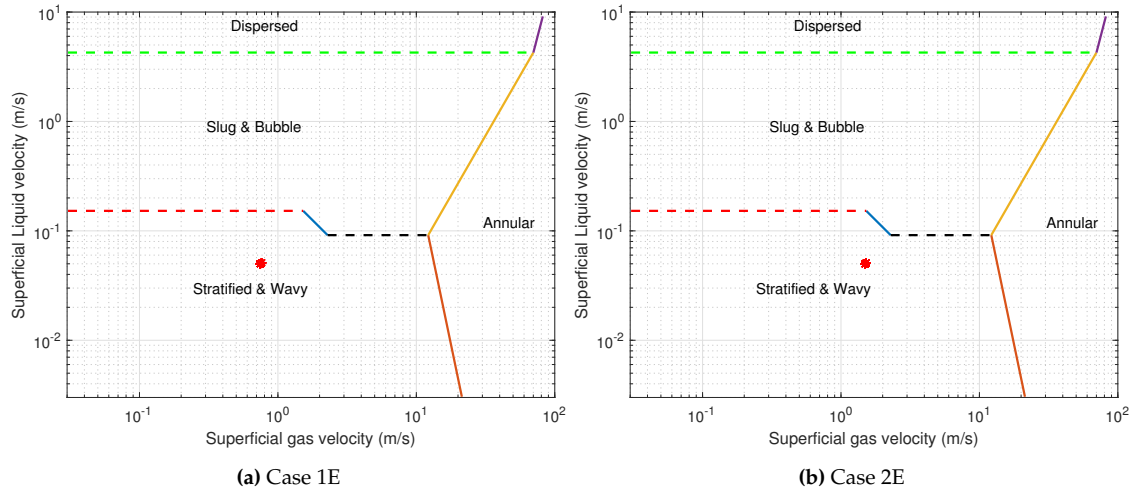


Figure 11.7: Flow pattern map - Cases 1&2 E/Em

Figure 11.7 shows a stratified & wavy flow pattern for main cases 1E and 2E. These results are in agreement with the flow pattern predictions done in OLGA[®].

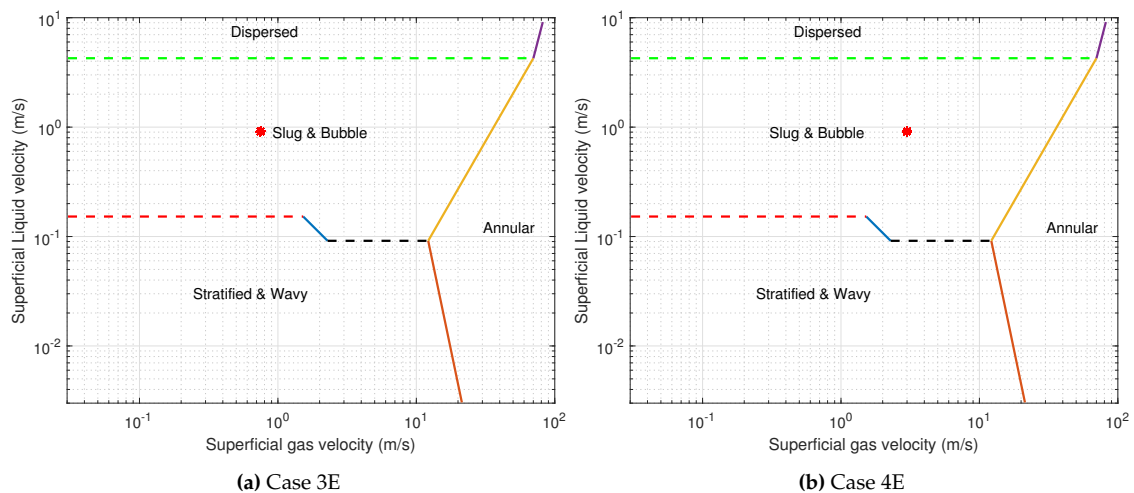


Figure 11.8: Flow pattern map - Cases 3&4 E/Em

Similarly, Fig.11.8 shows a slug & bubble flow pattern for main cases 3E and 4E. These results are in agreement with the flow pattern predictions done in OLGA[®].

These results demonstrate as well that the flow pattern prediction module in Matlab[®] is accurately developed, obtaining valid results.

11.2 Wax precipitation along the pipeline

This section presents the results regarding wax precipitation profiles obtained in Matlab[®]. The results for main cases 1E and 2E as well as for main cases 3E and 4E are shown in Figs.11.9 and 11.10, respectively. For each main case, the wax precipitation profile considering bulk and wall temperatures are shown for original wax characterization (WAT 46.5 °C) and modified wax characterization (WAT 35.5 °C).

Even though the wax precipitation profiles are calculated considering bulk and wall temperatures, the condition to begin with the wax precipitation calculations in the Matlab[®]

model states that the bulk temperature should be lower than the corresponding WAT value. This condition is considered based on the uncertainties related to wall temperature calculations presented in section 11.1.

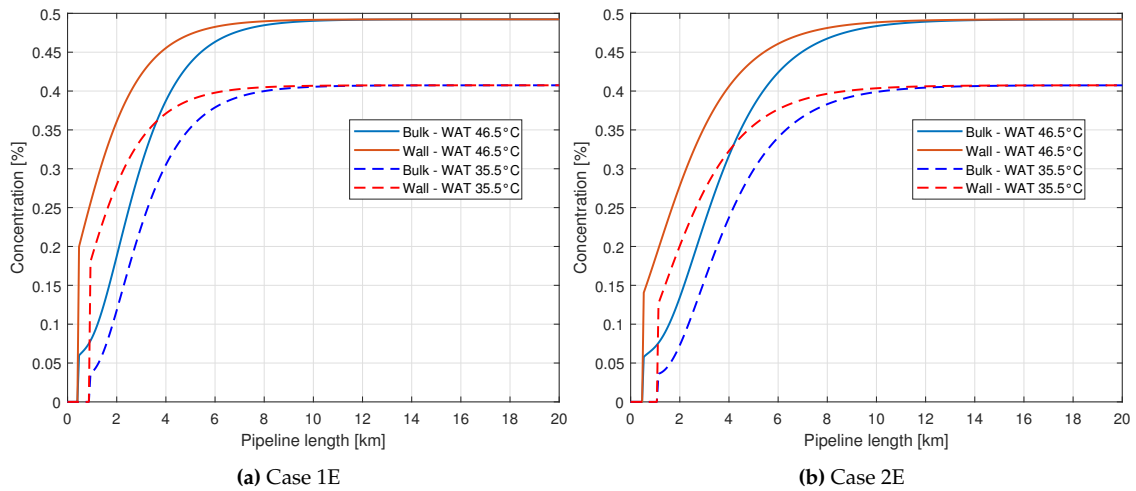


Figure 11.9: Wax precipitation curve - Cases 1&2 E/Em

The information provided by Fig.11.9 is closely related to Table 11.1 which presents the length of the pipeline where the WAT values are reached considering the two wax appearance temperatures (46.5 and 35.5 °C) analyzed in this project.

The trend followed by the wax precipitation profiles in both wax characterization scenarios is similar for cases 1E and 2E. The starting point for the formation of wax concurs with the length at which the bulk temperature reaches the corresponding WAT value (see Table 11.1). Similarly, the precipitation profiles for bulk and wall temperatures present an equal and asymptotic trend when the thermal equilibrium is reached at around 8 and 10 km for case 1E and 2E, respectively.

The concentration of wax obtained for the original wax characterization scenario presents higher values than the concentration regarding the modified wax characterization. This behavior is related to the two different equations used to calculate the wax precipitation (Eqs.10.10 and 10.11) when the original and modified wax characterization are used.

The shape presented by the precipitation curves obtained for bulk and wall temperatures is an important parameter to consider because the wax deposition phenomenon is mainly driven by the concentration gradient of the wax dissolved in oil in the bulk liquid and the wall surroundings. Generally speaking, for cases 1E and 2E, considering the original and modified wax composition, the difference between the concentration of precipitated wax obtained in the bulk liquid and the one obtained in the wall surroundings first increases reaching a maximum difference and then such difference decreases until it is equal to zero in the corresponding asymptote of the curve. Considering that the dissolved wax is obtained subtracting the precipitated wax from the wax content value (4.3% - Table 8.1) a similar behavior is followed by the difference between the dissolved wax at bulk and wall surroundings.

Figure 11.10 shows the results of bulk and wall wax precipitation profile related to cases 3E and 4E, considering the original (WAT 46.5 °C) and modified (WAT 35.5 °C) wax characterization.

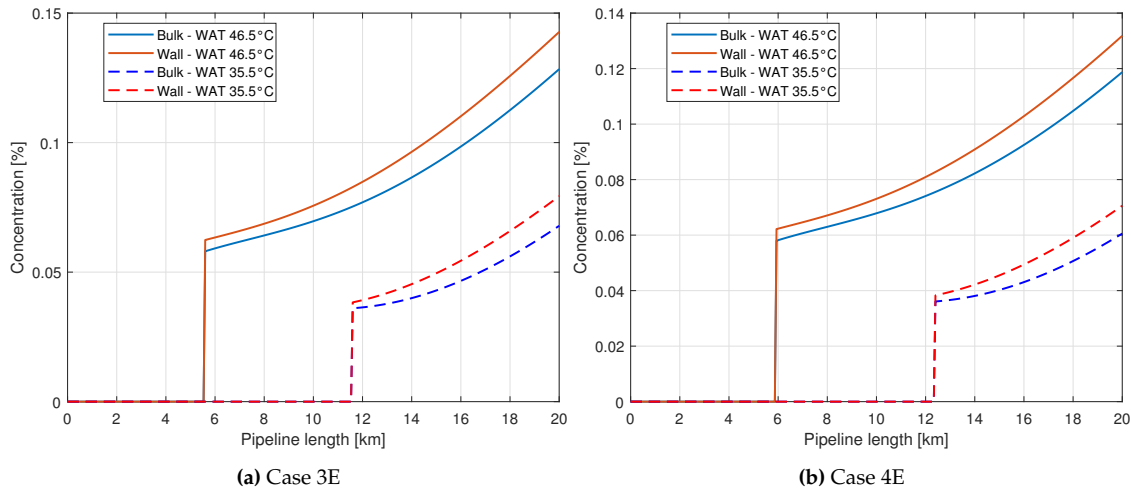


Figure 11.10: Wax precipitation curve - Cases 3&4 E/Em

The information provided by Fig.11.10 is closely related to Table 11.3 which presents the points where the WAT values are reached considering the two wax appearance temperatures (46.5 and 35.5 °C) analyzed in this project.

The trend followed by the wax precipitation profiles in both wax characterization scenarios is similar for cases 3E and 4E. The starting point for the formation of wax concurs with the length at which the bulk temperature reaches the corresponding WAT value (see Table 11.3).

Likewise to cases 1E and 2E, the concentration of wax obtained for the original wax characterization scenario presents higher values than the concentration regarding the modified wax characterization. This behavior is related to the two different equations used to calculate the wax precipitation (Eqs.10.10 and 10.11) when the original and modified wax characterization are used.

It is important to mention that for cases 3E and 4E, considering only the original wax composition, the difference between bulk and wall concentrations of precipitated wax first slightly decreases presenting a minimum difference, but then such difference increases along the pipeline. Similarly, the difference of the dissolved wax at bulk and wall surroundings follows the same trend. On the contrary, for the modified wax composition, the difference between bulk and wall concentrations of precipitated wax increases along the pipeline since its appearance.

Note that these calculations represent a very simplistic approach considered in Matlab[®] to model the thermodynamic process of wax formation. On the other hand, OLGA[®] uses Multiflash[®] to perform these computations through flash calculations and wax formation models.

11.3 Wax deposition

A comparative analysis of the results obtained in the commercial simulator OLGA[®] with the results of the code developed in Matlab[®] allows to have a better understanding of the wax deposition process and its prediction through mathematical models.

This section presents the results regarding wax deposition thickness along the pipeline

as well as its evolution through time considering the 16 study cases run in OLGA[®] and Matlab[®] code.

11.3.1 Wax deposition profile

This section presents the results regarding wax deposition thickness along the pipeline for the 16 study cases run in OLGA[®] and Matlab[®] code.

Figure 11.11 and Table 11.6 show the results of wax deposition thickness along the pipeline for the four study cases related to main case 1E.

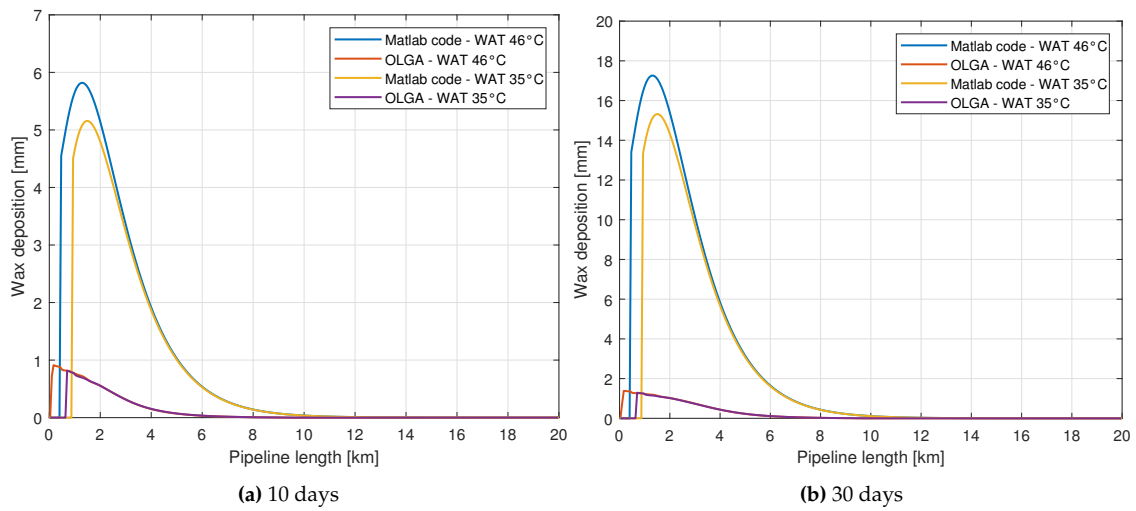


Figure 11.11: Wax deposition profile - Cases 1E & 1Em

Table 11.6: Wax deposition max. thickness and location - Cases 1E & 1Em

Study cases	10 days		30 days	
	Max. thickness	Location	Max. thickness	Location
1E-OLGA [®]	0.91	0.17	1.38	0.17
1E-Matlab [®]	5.82	1.33	17.26	1.33
1Em-OLGA [®]	0.82	0.70	1.28	0.70
1Em-Matlab [®]	5.16	1.51	15.32	1.53

Max. thickness is expressed in *mm* and Location in *km*

In general, OLGA[®] predicts the first point for the wax deposition when the WAT is reached by the wall temperature. On the other hand, Matlab[®], as coded, presents its first point for wax deposition when the WAT is reached by the bulk temperature. Due to the uncertainties observed in wall temperature calculations in Matlab[®], the bulk temperature was selected as parameter for estimation of the wax formation point through the WAT. However, for the current case, both codes present similar starting points for wax deposition. Similarly, comparing the original and modified wax characterization, the initial points for wax deposition do not present significant differences; in other words, for the main case 1E the modified characterization can be used in the simulation of wax deposition presenting results closely similar to the ones obtained with the original wax characterization regarding the position in the pipeline where wax deposition appears.

Overall, the modified characterization presents slightly lower results regarding wax deposition thickness in OLGA[®] and Matlab[®]; thus, the modified characterization can be used instead of the original one without major differences in the results of wax deposition thickness.

Matlab[®] over predicts the thickness of the wax deposited around five to ten times for 10 and 30 days respectively, compared to the results obtained through OLGA[®]. This over prediction is mainly due to the higher difference between bulk and wall temperature that Matlab[®] presents instead of OLGA[®]. Additionally, OLGA[®] calculates an overall heat transfer coefficient (OHTC) that changes as a consequence of the increment in the thickness of the wax precipitation layer reducing the driven force of the wax deposition phenomenon regarding temperature gradient. As noted before, the code in Matlab[®] considers the OHTC constant for all the calculations. From another perspective, when the two wax characterizations are used in the same simulation tool, either OLGA[®] or Matlab[®], the results do not present significant differences between each other.

OLGA[®] presents a maximum wax deposition thickness at the beginning of the wax layer, which agrees with the highest temperature difference between the bulk and wall temperatures presented in the first sections of the pipeline. Such temperature difference decreases until becoming zero when the thermal equilibrium is reached. The same decreasing trend is presented by the wax deposit profile as expected, which is shown in OLGA[®] results. However, the Matlab[®] code presents a first big wax thickness at the beginning of the layer, then the wax profile increases until a maximum value is reached and later it reduces progressively to zero. This behavior is explained in section 11.2 for the difference for dissolved wax between the bulk liquid and the wall surroundings which seems to be the responsible for the shape presented by the deposit wax layer. Overall, this behavior is an additional factor for the wax thickness over prediction obtained with Matlab[®].

Figure 11.12 and Table 11.7 show the results of wax deposition thickness along the pipeline for the four study cases related to main case 2E.

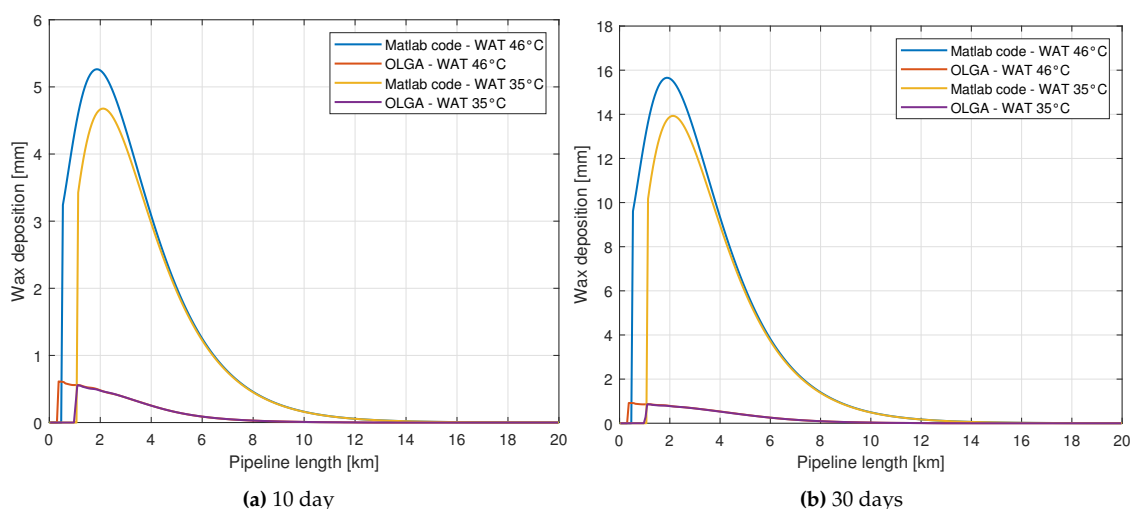


Figure 11.12: Wax deposition profile - Cases 2E & 2Em

As observed, a behavior similar to the main case 1E is obtained for the main case 2E. Thus, the discussion previously developed for the main case 1E correctly applies to the results of main case 2E. Consequently, it might be appropriate to consider that the wax deposition behavior when the fluid follows a stratified flow pattern results in the profile

Table 11.7: Wax deposition max. thickness and location - Cases 2E & 2Em

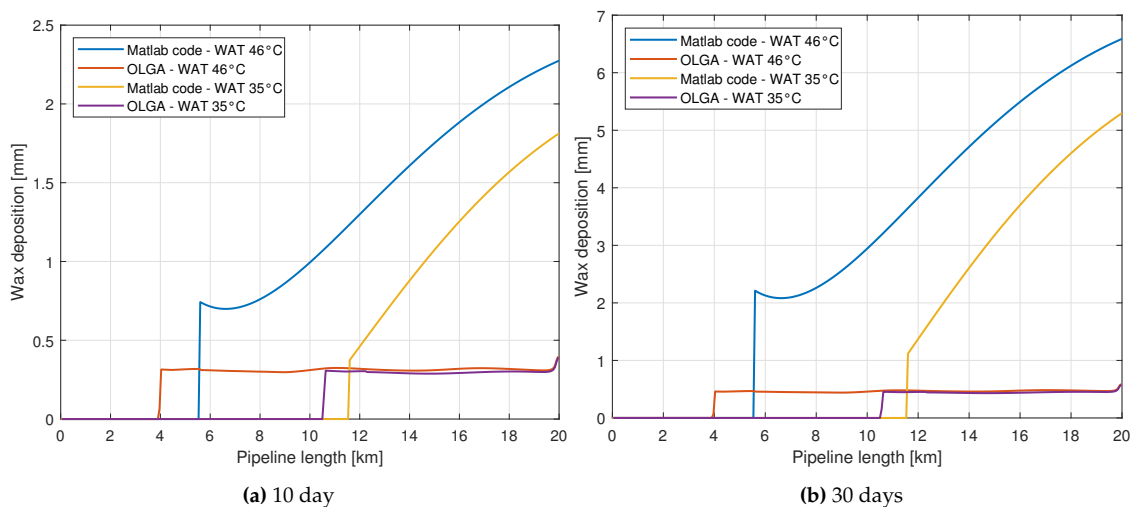
Study cases	10 days		30 days	
	Max. thickness	Location	Max. thickness	Location
2E-OLGA [®]	0.61	0.37	0.92	0.37
2E-Matlab [®]	5.26	1.87	15.66	1.87
2Em-OLGA [®]	0.56	1.10	0.86	1.10
2Em-Matlab [®]	4.67	2.13	13.93	2.13

Max. thickness is expressed in *mm* and Location in *km*

presented in cases 1E and 2E, if the heat transfer phenomenon presents strong similarities with the one observed in the present project for the corresponding cases.

Additionally, in OLGA[®] as well as Matlab[®], it is observed that the maximum thickness of the wax deposition layer decreases as the gas mass flow increases. It is possible to infer that the increased mass flow reduces the temperature difference between bulk and wall temperatures, and consequently reduces the concentration difference of wax dissolved in the liquid bulk and the wall surroundings producing a lower driven force for the wax deposition phenomenon.

Figure 11.13 and Table 11.8 show the results of wax deposition thickness along the pipeline for the four study cases related to main case 3E.

**Figure 11.13:** Wax deposition profile - Cases 3E & 3Em**Table 11.8:** Front wax deposition thickness and location - Cases 3E & 3Em

Study cases	10 days		30 days	
	Front thickness	Location	Front thickness	Location
3E-OLGA [®]	0.31	4.03	0.46	4.03
3E-Matlab [®]	0.74	5.60	2.21	5.06
3Em-OLGA [®]	0.30	10.63	0.45	10.63
3Em-Matlab [®]	0.38	11.60	1.12	11.60

Front thickness is expressed in *mm* and Location in *km*

In general, OLGA[®] predicts the first point for the wax deposition when the WAT is reached by the wall temperature. On the other hand, Matlab[®], as coded, presents its first point for wax deposition when the WAT is reached by the bulk temperature; as a consequence, the wax deposit predicted by OLGA[®] appears first in the pipeline. Additionally, comparing the original and modified wax characterization, the initial points for wax deposition change drastically using both simulation tools; in other words, under conditions of main case 3E the modified and the original wax characterization cannot be used interchangeably because a difference around 6 km is presented in the appearance of the wax layer.

Overall, the modified characterization presents lower results regarding wax deposition thickness in Matlab[®] while the wax deposition thickness in OLGA[®] is practically the same; thus, the modified characterization can be used instead of the original one without major differences in the results of wax deposition thickness when using OLGA[®].

Matlab[®] over predicts the thickness of the wax deposited in ratios lower than 6 times for 10 days and 13 times for 30 days. This over prediction is mainly due to the shape presented by the difference between the concentration of the wax dissolved in the bulk liquid and the wall surroundings, as explained in section 11.2, which is the responsible for the shape presented by the deposit wax layer. These results let us understand the high sensitivity of the Matlab[®] code to the equation used to describe the thermodynamics of the wax formation. On the other hand, OLGA[®] uses flash calculations and wax models to perform in an accurate way the thermodynamics regarding wax precipitation phenomenon.

From another perspective, when the two wax characterizations are used in the same simulation tool, either OLGA[®] or Matlab[®], the results do not present significant differences between each other regarding wax thickness predictions; however, the modified and the original wax characterization cannot be used interchangeably for predictions of the wax deposit position in the pipeline.

OLGA[®] presents a constant wax deposition thickness along the entire length of the wax layer, which agrees with the almost constant temperature difference between the bulk and wall temperatures presented along all sections of the pipeline. Thus, it is expected that this constant temperature difference should be translated to a constant concentration difference of dissolved wax between the bulk fluid and the wall surrounding, which at the end results in a constant deposited wax layer. However, considering the original wax characterization, the Matlab[®] code presents a first front of wax thickness at the beginning of the layer, then the wax profile decreases until a minimum value is reached and later it increases progressively along the pipeline. On the other hand, considering the modified wax characterization, the Matlab[®] code presents an increasing profile along the pipeline from the wax layer appearance. These behaviors are explained in section 11.2 for the difference of dissolved wax between the bulk liquid and the wall surroundings which seems to be the responsible for the shape presented by the deposit wax layer.

Figure 11.14 and Table 11.9 show the results of wax deposition thickness along the pipeline for the four study cases related to main case 4E.

As observed, a behavior similar to the main case 3E is obtained for the main case 4E. Thus, the discussion previously developed for the main case 3E correctly applies to the results of main case 4E. Consequently, it might be appropriate to consider that the wax

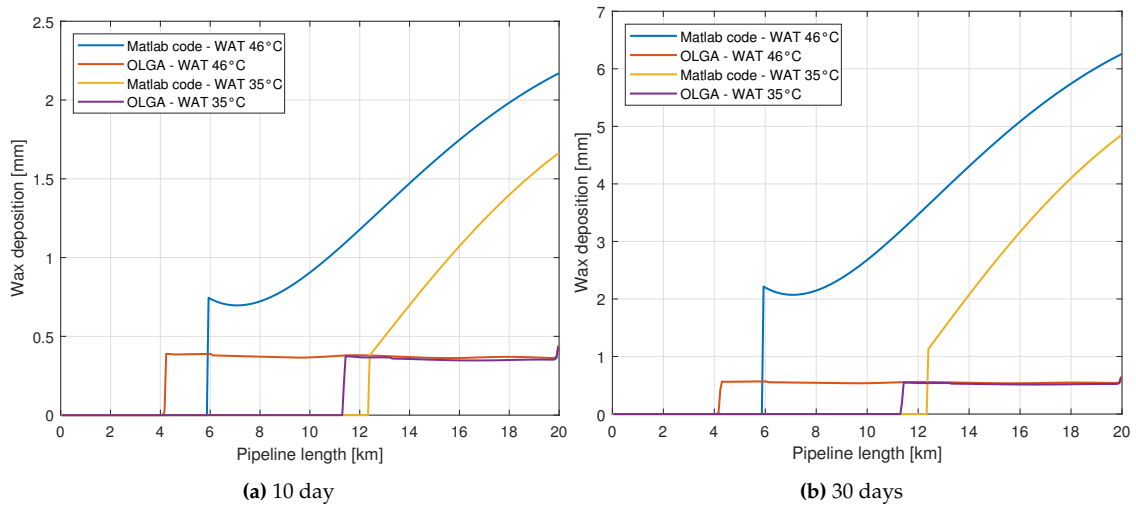


Figure 11.14: Wax deposition profile - Cases 4E & 4Em

Table 11.9: Front wax deposition max. thickness and location - Cases 4E & 4Em

Study cases	10 days		30 days	
	Front thickness	Location	Front thickness	Location
4E-OLGA [®]	0.39	4.23	0.56	4.30
4E-Matlab [®]	0.75	5.93	2.22	5.93
4Em-OLGA [®]	0.37	11.43	0.55	11.50
4Em-Matlab [®]	0.38	12.30	1.13	12.40

Front thickness is expressed in *mm* and Location in *km*

deposition behavior when the fluid follows a slug flow pattern results in the profile presented in cases 3E and 4E, if the heat transfer phenomenon presents strong similarities with the one observed in the present project for the corresponding cases.

Additionally, in OLGA[®] as well as Matlab[®] comparing cases 3E and 4E, it is observed that the starting point of the appearance of the wax layer is moved further in the pipeline when the gas mass flow increases. This can be explained considering that WAT is reached by the fluid temperature further in the pipeline for cases 4E.

Generally speaking, comparing the wax deposition behavior for study cases which present stratified flow (1E & 2E) with study cases that show a slug pattern flow (3E & 4E), an important difference is observed regarding the thickness of the deposited wax layer. The latter cases present notorious lower thickness of the wax layer due to smaller temperature difference and consequently wax concentration differences between the bulk fluid and wall surroundings; additionally, the stripping effect on the wax deposition thickness due to the slug flow causes a reduction of the thickness of the wax deposit layer.

11.3.2 Wax deposition evolution through time

This section presents the results regarding wax deposition thickness trend through time for the 16 study cases run in OLGA[®] and Matlab[®] code.

In the study cases related to main cases 1E and 2E, the analyses of the wax deposition evolution through time are performed considering the maximum layer thickness point,

according to information presented in Tables 11.6 and 11.7. On the other hand, for study cases related to main cases 3E and 4E, the wax evolution analyses are done for the front or first point where the wax deposition appears, as presented in Tables 11.8 and 11.9.

Figure 11.15 shows the results of wax deposition thickness evolution for the four study cases related to main case 1E.

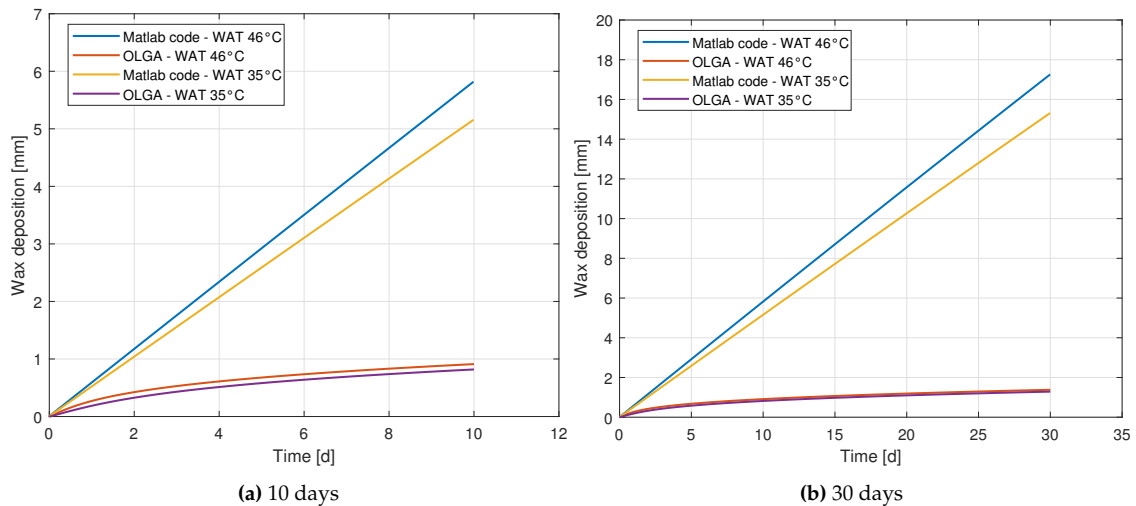


Figure 11.15: Wax deposition trend - Case 1E & 1Em

In general, OLGA[®] presents an exponential-like trend for wax deposition growing in the point that shows the maximum wax layer thickness. This behavior is related to the constant changes experienced by the heat transfer phenomenon through time. These changes are related to the fact that wax is continuously deposited on the inner surface of the pipe affecting the overall heat transfer coefficient (OHCT) and consequently reducing the difference between the bulk and wall temperatures. Moreover, it is important to understand that a new inner wax layer covers the wall surface and the previously deposited layers producing a thermal isolating effect. So, this reduces the temperature difference between the bulk and the new inner surface of the pipeline producing a reduction in the driven force of the wax deposition phenomena.

The aforementioned exponential-like trend followed by OLGA[®] can be easily visualized in the results regarding 30 days of deposition time because the growing trend presents a stronger asymptotic behavior after 10 days of deposition.

On the other hand, the Matlab[®] code considers a constant OHCT values. This consideration produces deposit trends that follow a linear-like pattern.

The deposited layer thickness over prediction resulting of the Matlab[®] code, which is discussed in section 11.3, is well observed in Fig.11.15.

Figure 11.16 shows the results of wax deposition thickness evolution for the four study cases related to main case 2E.

As observed, a behavior similar to the main case 1E is obtained for the main case 2E. Thus, the discussion previously developed for the main case 1E correctly applies to the results of main case 2E.

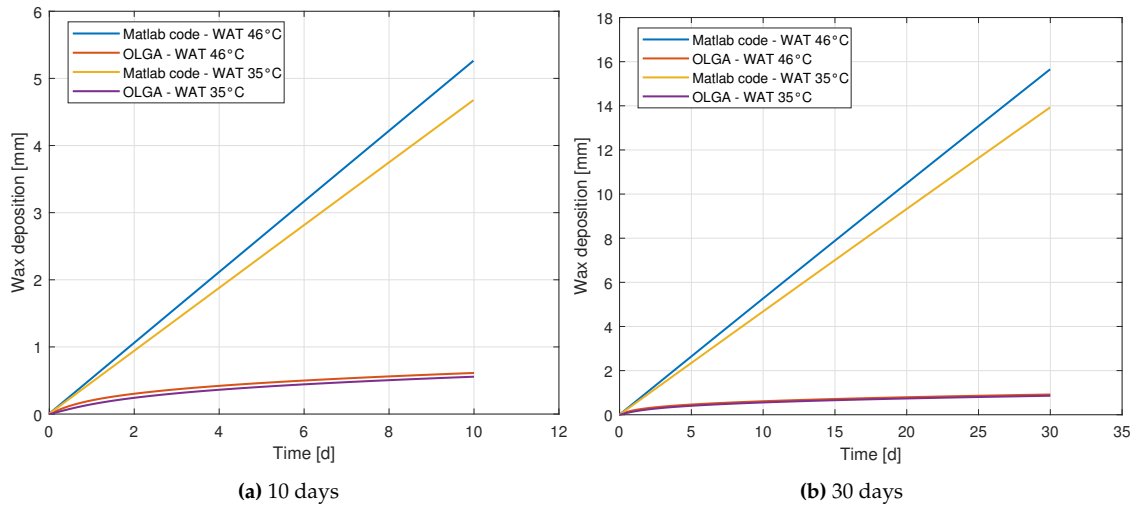


Figure 11.16: Wax deposition trend- Case 2E & 2Em

As previously stated, in OLGA[®] as well as Matlab[®], it is observed that the maximum thickness of the wax deposition layer decreases as the gas mass flow increases.

Figure 11.17 shows the results of wax deposition thickness evolution for the four study cases related to main case 3E.

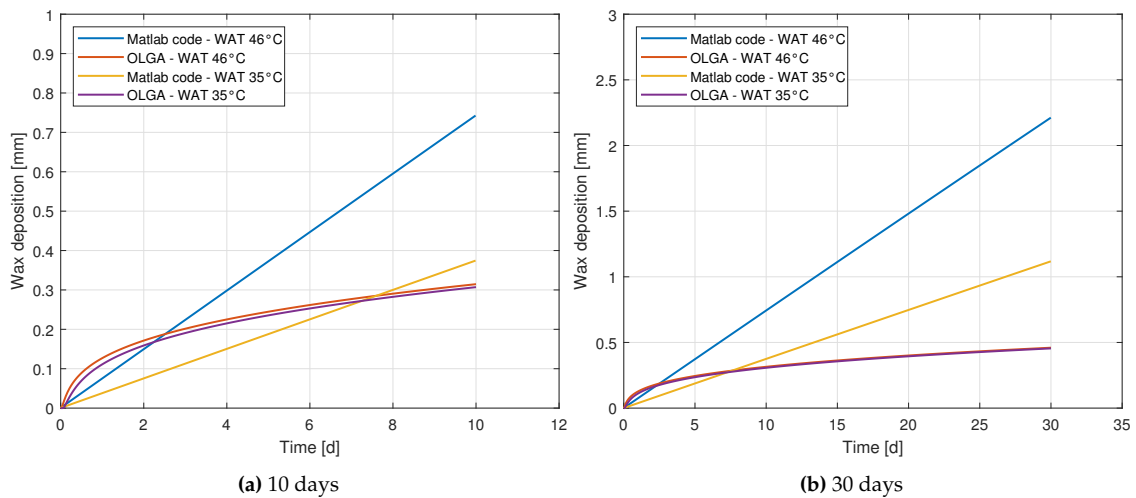


Figure 11.17: Wax deposition trend- Case 3E & 3Em

The analysis presented for the study cases related to the main case 3E considers the growing behavior of the point where the wax layer starts to appear in the pipeline or the front of the wax deposition layer. Using this approach, the results obtained from OLGA[®] and Matlab[®] are compared considering that the increasing wax deposition shape obeys to the simplistic thermodynamic information provided to the Matlab[®] code.

As observed, a behavior similar to the main cases 1E and 2E is obtained for the main case 3E. Thus, the discussion previously developed for the main cases 1E and 2E correctly applies to the results of main case 3E. However, in case 3E the over prediction of the deposited layer thickness resulting of the Matlab[®] code, observed in Fig.11.17, is lower and presents closer values to OLGA[®] results.

Figure 11.18 shows the results of wax deposition thickness evolution for the four study

cases related to main case 4E.

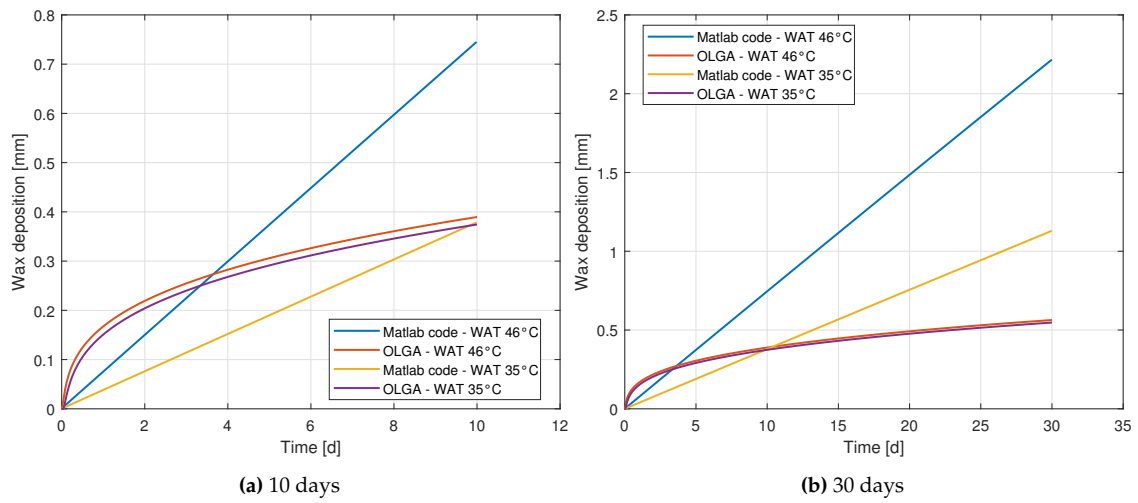


Figure 11.18: Wax deposition trend- Case 4E & 4Em

As observed, a behavior similar to the main case 3E is obtained for the main case 4E. Thus, the discussion previously developed for the main case 3E correctly applies to the results of main case 4E.

12 Conclusions

The Matlab[®] self developed code over predicts the thickness of the wax deposited layer around five to ten times compared to the results obtained through OLGA[®]. This over prediction can be attributed to the higher difference between values of bulk and wall temperature when the flow presents a stratified pattern, and the trend followed by the difference of the concentration of the dissolved wax between the bulk fluid and the wall surroundings when the flow presents a slug pattern.

Even with the wax thickness over prediction the results can be considered acceptable as a first approximation of the wax deposition phenomenon based on the fact that more conservative results are obtained through the Matlab[®] self developed code.

An accurate heat transfer modeling, which includes the wall temperature calculations considering the multiphase characteristic of the fluid as well as an updating OHTC estimation that considers every new wax layer deposited in the inner surface of the pipeline, plays a critical role in the wax deposition simulation for multiphase flow in pipelines.

The thermodynamic approach used for the analysis of the wax deposition formation is a basic parameter to accurately calculate the dissolved wax concentration avoiding wrong predictions of wax deposition.

A representative wax characterization regarding wax appearance temperature is directly linked with the prediction of wax deposition and consequently with the location of the deposited wax layer.

13 Future work

Future projects can be developed considering as a starting point the present work.

A multiphase heat transfer module together with a wax deposition thermodynamic module can be implemented in order to increase the accuracy of the self developed wax deposition model.

Additionally, to run real case scenarios, a pressure drop determination module as well as a multiphase flow pattern module for vertical pipelines can be implemented in the self developed code built in the present project.

A better understanding of the WAT determination for waxy oils can be done through an experimental study using the different techniques to estimate the wax appearance temperature.

Bibliography

- [1] K. Pedersen, P. Christensen, and J. Shaikh, *Phase Behavior of Petroleum Reservoir Fluid*. CRC Press, 2015. ISBN 13: 978-1-4398-5227-9.
- [2] M. S. Apte, A. Matzain, H. Q. Zhang, M. Volk, J. P. Brill, and J. L. Creek, "Investigation of paraffin deposition during multiphase flow in pipelines and wellbores - Part 2: Modeling," *SPE Reprint Series*, vol. 123, no. 58, pp. 171–178, 2004.
- [3] A. Aiyejina, D. P. Chakrabarti, A. Pilgrim, and M. K. Sastry, "Wax formation in oil pipelines: A critical review," *International Journal of Multiphase Flow*, vol. 37, no. 7, pp. 671–694, 2011.
- [4] Y. Bai and Q. Bai, *Subsea pipelines and risers*. Elsevier, 2005. ISBN: 0-080-4456-67.
- [5] R. Venkatesan, N. Nagarajan, K. Paso, Y.-B. Yi, A. Sastry, and H. Fogler, "The strength of paraffin gels formed under static and flow conditions," *Chemical Engineering Science*, vol. 60, no. 13, pp. 3587 – 3598, 2005.
- [6] O. Skjæraasen, H. J. Oschmann, K. Paso, and J. Sjöblom, "Accurate assessment of pipeline restart behavior at subsea conditions for a highly waxy crude oil employing advanced computational pressure wave modeling," *Industrial and Engineering Chemistry Research*, vol. 54, no. 16, pp. 4429–4440, 2015.
- [7] J. J. Barrera Escobedo, A. O. Nieckele, and L. F. A. Azevedo, "Analysis of the Transient Cooldown of Sub-Sea Pipelines," vol. Volume 1: Project Management; Design and Construction; Environmental Issues; GIS/Database Development; Innovative Projects and Emerging Issues; Operations and Maintenance; Pipelining in Northern Environments; Standards and Regulations, pp. 845–853, 09 2006.
- [8] C. Van Der Geest, V. C. Guersoni, and A. C. Bannwart, "Experimental study of the time to restart the flow of a gelled waxy crude in rheometer and pipeline," *Journal of Petroleum Science and Engineering*, vol. 181, no. July, p. 106247, 2019.
- [9] R. Bagatin, C. Carniani, S. Corraera, M. Margarone, and C. Busto, "Wax modeling: There is need for alternatives," 2008. SPE-115184-MS.
- [10] G. Giacchetta, B. Marchetti, M. Leporini, A. Terenzi, D. Dall'Acqua, L. Capece, and R. Cocci Grifoni, "Pipeline wax deposition modeling: A sensitivity study on two commercial software," *Petroleum*, vol. 5, no. 2, pp. 206–213, 2019.
- [11] M. Leporini, A. Terenzi, B. Marchetti, G. Giacchetta, and F. Corvaro, "Experiences in numerical simulation of wax deposition in oil and multiphase pipelines: Theory versus reality," *Journal of Petroleum Science and Engineering*, vol. 174, no. February 2018, pp. 997–1008, 2019.

-
- [12] I. Noville and L. Naveira, "Comparison between real field data and the results of wax deposition simulation," 2012. SPE-152575-MS.
- [13] C. Labes-Carrier, H. P. Rønningsen, J. Kolnes, and E. Leporcher, "Wax deposition in north sea gas condensate and oil systems: Comparison between operational experience and model prediction," 2002. SPE-77573-MS.
- [14] A. Singh, H. S. Lee, P. Singh, and C. Sarica, "Flow Assurance: Validation of Wax Deposition Models Using Field Data from a Subsea Pipeline," 2011.
- [15] Y. Chi, "Wax deposition under two-phase gas-oil stratified flow," 2019. PhD Thesis.
- [16] K. Døble, "Wax deposition as a function of flow," 2018. Master's Thesis.
- [17] J. S. Gudmundsson, *Flow Assurance Solids in Oil and Gas Production*. CRC Press, 2018. ISBN: 978-1-138-73784-6.
- [18] Z. Huang, S. Zheng, and H. S. Fogler, *Wax Deposition - Experimental Characterizations, Theoretical Modeling, and Field Practices*. CRC Press, 2015. ISBN 13: 978-1-4665-6767-2.
- [19] H. P. Roenningsen, B. Bjoerndal, A. Baltzer Hansen, and W. Batsberg Pedersen, "Wax precipitation from north sea crude oils: 1. crystallization and dissolution temperatures, and newtonian and non-newtonian flow properties," *Energy & Fuels*, vol. 5, no. 6, pp. 895–908, 1991.
- [20] D. Tiwary and A. K. Mehrotra, "Phase transformation and rheological behaviour of highly paraffinic "waxy" mixtures," *The Canadian Journal of Chemical Engineering*, vol. 82, no. 1, pp. 162–174, 2004.
- [21] B. Edmonds, T. Moorwood, R. Szczepanski, and X. Zhang, "Simulating wax deposition in pipelines for flow assurance," *Energy & Fuels*, vol. 22, no. 2, pp. 729–741, 2008.
- [22] J. A. Svendsen, "Mathematical modeling of wax deposition in oil pipeline systems," *AIChE Journal*, vol. 39, no. 8, pp. 1377–1388, 1993.
- [23] O. Bratland, *Multi-phase Flow Assurance - Pipe Flow 2*. 2013. ISBN: 978-616-335-926-1.
- [24] G. Yadigaroglu and G. F. Hewitt, *Introduction to Multiphase Flow - Basic Concepts, Application and Modelling*. Springer, 2018. ISBN: 978-3-319-58718-9.
- [25] J. Mandhane, G. Gregory, and K. Aziz, "A flow pattern map for gas—liquid flow in horizontal pipes," *International Journal of Multiphase Flow*, vol. 1, no. 4, pp. 537 – 553, 1974.
- [26] A. Matzain, "Multiphase flow paraffin deposition modeling," 1999. PhD Thesis.
- [27] A. Matzain, M. S. Apte, H.-Q. Zhang, M. Volk, J. P. Brill, and J. L. Creek, "Investigation of Paraffin Deposition During Multiphase Flow in Pipelines and Wellbores—Part 1: Experiments ," *Journal of Energy Resources Technology*, vol. 124, pp. 180–186, 08 2002.
- [28] A. Rittirong, "Paraffin deposition under two-phase gas-oil slug flow in horizontal pipes," 2014. PhD Thesis.
- [29] K. Rosvold, "Wax deposition models," 2008. Master's Thesis.

-
- [30] C. R. Wilke and P. Chang, "Correlation of diffusion coefficients in dilute solutions," *AIChE Journal*, vol. 1, no. 2, pp. 264–270, 1955.
- [31] K. K. Botne, "Modeling wax thickness in single-phase turbulent flow," 2012. Master's Thesis.
- [32] Schlumberger, "Olga user manual," 2019.
- [33] Schlumberger, "Olga user manual," 2016. Version 2016.2.
- [34] B. J. Musser and P. K. Kilpatrick, "Molecular characterization of wax isolated from a variety of crude oils," *Energy & Fuels*, vol. 12, no. 4, pp. 715–725, 1998.
- [35] H. M. B. Veiga, F. P. Fleming, and L. F. A. Azevedo, "Wax deposit thermal conductivity measurements under flowing conditions," *Energy & Fuels*, vol. 31, no. 11, pp. 11532–11547, 2017.
- [36] M. M. El-Dalatony, B.-H. Jeon, E.-S. Salama, M. Eraky, W. B. Kim, J. Wang, and T. Ahn, "Occurrence and characterization of paraffin wax formed in developing wells and pipelines," *Energies - MDPI*.
- [37] I. Tosun, *Modeling in Transport Phenomena: A Conceptual Approach*. Elsevier Science B.V., 2007.
- [38] L. C. Maley and W. P. Jepson, "Liquid holdup in large diameter horizontal multiphase pipelines," *The American Society of Mechanical Engineers - Petroleum Division*.
- [39] N. Lindeloff and K. Krejbjerg, "A compositional model simulating wax deposition in pipeline systems," *American Chemical Society - Energy and Fuels*.

Appendix

Code developed in Matlab[®] for wax deposition analysis

MAIN CODE

```
clear all
close all
clc
```

Inputs

```
%----- Fluid flow and Properties -----
CpL = 2.074;          %[kJ/kg-K] - Heat capacity of liquid fraction
rhoL = 822.74;       %[kg/m3]   - Liquid density
muL = 0.003;        %[Pa.s]    - Dynamic viscosity
sigmaL = 0.01625;   %[N/m]     - Liquid surface tension
tkL = 0.18;         %[W/m-K]   - Liquid thermal conductivity

CpG = 2.357;        %[kJ/kg-K] - Heat capacity of vapor fraction
rhoG = 18.41;       %[kg/m3]   - Gas density
muG = 0.000012;    %[Pa.s]    - Dynamic viscosity
tkG = 0.04;        %[W/m-K]   - Liquid thermal conductivity

mwW = 475;          %[g/mol]    - Wax molecular weight
rhoW = 0.9;         %[g/cm3]   - Wax density 900[kg/m3]

%----- Temperature and pressure -----
T_amb = 5;          %[C]       - Ambient temperature
T_in = 60;          %[C]       - Inlet temperature
P_out = 2204254;    %[Pa]      - Inlet pressure

%----- Process and pipe characteristics -----
U = 20;             %[W/m2-K] - System overall heat transfer coeff

d_0 = 1;            %[m]       - Pipe inner diameter
L = 20000;          %[m]       - Pipe length
k = 4.572E-5;       %[m]       - Pipe roughness
tkW = 45;           %[W/m-K] - Pipe thermal conductivity

%+++++ VARIABLE INPUTS +++++
mL = 591.35;        %[kg/s]    - Liquid mass flow
mG = 11.14;         %[kg/s]    - Gas mass flow
ni = 300;           %[-]       - Number of pipeline segments

WAT_0 = 46.5;       %[C]       - Wax Appearance Temperature
% WAT_0 = 35.5;     %[C]       - Wax Appearance Temperature

%----- Wax deposition parameters -----
C1 = 15;            %[-]       - Enhancement due to wax porosity
C2 = 0.055;         %[-]       - Reduction due to shear stripping
C3 = 1.4;           %[-]       - Reduction due to shear stripping

t_final = 10 ;      %[d]       - Final time for wax evaluation
```

```

time_step = 1000 ; %[s] - Time step for wax deposition evaluation
deltaW_0 = 0;      %[mm] - Value for initial deposition

%----- Precalculation -----
[m_tot, alphaL, WAT, d, CpM, rhoM, muM, tkM, dx, x, t_end, nj, deltaW, nq, timeWAX, ...
timeCOOLING] = Precalc(mL, mG, WAT_0, d_0, CpL, CpG, rhoL, rhoG, muL, muG, ...
tkL, tkG, ni, L, t_final, deltaW_0, time_step, cool_time, cool_step);

%----- Calling functions -----

for j = 1:nj
%----- Bulk temperature -----
[Tb] = BulkTemp(T_in, T_amb, U, d, m_tot, CpM, dx, x, ni);

%----- Pressure drop -----
[DeltaPres, v] = PDrop(rhoL, m_tot, d, muL, k, x, P_out, ni);

%----- Multiphase regime determination - Mandhane -----
[regimeMan, usL, usG, regM, alertM] = FlowRegMan(rhoL, rhoG, alphaL, m_tot, d, ni);

%----- Multiphase regime map Mandh -----
[usG3, usG5, usG6, usG7, usL1, usL2, usL3, usL4, usL5, usL6, usL7, usG1_1, usG1_2, ...
usG2_1, usG2_2, usG4_1, usG4_2] = RegMapMan(usL, usG);

%----- Wall temperature -----
[Twi, Two, ReL, alertRe, PrL, alertPr, h_in] = WallTemp(Tb, T_amb, U, rhoM, muM, ...
CpM, tkM, tkW, usG, usL, d, ni, L, alphaL, m_tot);

%----- Wax solubility calculation -----
[SolBulk, SolWall, SolubDiff, ConcGrad] = Solubility(Tb, Twi, WAT, ni, WCont);

%----- Wax deposition calculation -----
[deltaWnew, dnew] = WaxDepo(mwW, rhoW, rhoL, muL, usL, usG, Tb, Twi, SolubDiff, ...
h_in, tkL, d, regimeMan, time_step, C1, C2, C3, deltaW, rhoM, ni, ConcGrad);

d = dnew;
deltaW = deltaWnew ;

end

```

PRE-CALCULATIONS

```
function [m_tot, alphaL, WAT, d, CpM, rhoM, muM, tkM, dx, x, t_end, nj, deltaW...
, nq, timeWAX, timeCOOLING] = Precalc(mL, mG, WAT_0, d_0, CpL, CpG, rhoL, ...
rhoG, muL, muG, tkL, tkG, ni, L, t_final, deltaW_0, time_step, ...
cool_time, cool_step)

%----- Total mass and fractions -----
m_tot = mL + mG;           %[kg/s] - Liquid mass porcentaje
alphaL = mL/(mL+mG);      "[%] - Liquid mass porcentaje

%----- WAT as vector -----
WAT = (WAT_0 + 273.15)*ones(1,ni+1);

%----- Diameter as vector -----
d = d_0*ones(1,ni+1);

%----- First wax depo as vector -----
deltaW = deltaW_0*ones(1,ni+1);

%----- Mixture properties -----
CpM = alphaL*CpL + (1-alphaL)*CpG;
rhoM = alphaL*rhoL + (1-alphaL)*rhoG;
muM = alphaL*muL + (1-alphaL)*muG;
tkM = alphaL*tkL + (1-alphaL)*tkG;

%----- Defining the grid -----
dx = L/ni;                 %[m] - Segment length
x = 0:dx:L;                %[-] - Grid points

%----- Pseudo Steady State INPUTS -----
t_end = t_final*3600*24 ;   %[s] - Final time for wax evaluation
nj = t_end/time_step ;     %[-] - Number of evaluation throug time
timeWAX = 1:time_step:t_end;

end
```

BULK TEMPERATURE

```
function [Tb] = BulkTemp(T_in, T_amb, U, d, m_tot, CpM, dx, x, ni)
%----- Changing values to SI -----
T_amb = T_amb + 273.15;    %[K]
T_in = T_in + 273.15;    %[K]
CpM = CpM*1000;          %[J/kg-K] - Mixture heat capacity

%----- Initializing the grid -----
T1 = zeros(1, ni);      %[-] - Temperature grid points
T2 = zeros(1, ni);      %[-] - Temperature grid points

%----- Setting inlet temperature -----
T1(1,1) = T_in;
T2(1,1) = T_amb + (T1(1,1) - T_amb)*exp((-U*pi*d(1,2)*dx)/(m_tot*CpM));

%----- Calculating -----
for i=2:ni
T1(1,i) = T2(1,i-1) ;
T2 = T_amb + (T1-T_amb)*exp((-U*pi*d(1,i)*dx)/(m_tot*CpM));
end

Tb = zeros(1, length(x));
Tb(1,1) = T1(1,1);
Tb(1,2:length(x)) = T2;
end
```

WALL TEMPERATURE

```
function [Twi,Two,ReL,alertRe,PrL,alertPr,h_in] = WallTemp(Tb,T_amb,U,...
rhoM,muM,CpM,tkM,tkW,m_tot,d,ni,L)
%----- Changing values to SI -----
T_amb = T_amb + 273.15;      %[K]
CpM = CpM*1000;            %[J/kg-K] - Heat capacity

%----- Previous calculations -----
% Considerning one homogeneous phase only
A = pi/4*d.^2;              %[m2] - Cross sectional area
QM = m_tot/rhoM;           %[m3/s] - Volume flow for one homogeneous mixture
vM = QM./A ;               %[m/s] - Velocity for one homogeneous mixture

%----- Calculating -----
ReL = rhoM*vM.*d./muM;
PrL = CpM*muM/tkM;

for i=1:ni+1
if ReL(i) < 2030
NuL = 1.86*(ReL(i).*PrL*d/L)^(1/3);
else
if ReL(i) >= 2300 && ReL(i) < 10000 && PrL <= 592
NuL = 0.0015*ReL(i).^0.83*PrL^0.42; %Whitaker
else
if ReL(i) >= 10000 && PrL <= 160
NuL = 0.023*ReL(i).^0.8*PrL^0.3; %Dittus-Boelter

elseif ReL(i) >= 10000 && PrL <= 16700 && PrL >= 160
NuL = 0.027*ReL(i).^(4/5)*PrL^(1/3); %Sieder-Tate
end
end
end

% Internal transfer coeff-resistance
h_in = NuL.*tkM./d;
R_in = 1./h_in;

%----- Wall temperatures calculations -----
HeatFlux = U*(Tb-T_amb);
Twi = Tb - HeatFlux.*R_in;

R_W = d./(2*tkW)* log((d.*1000/2+d.*39.37)/(d.*1000/2));
Two = Twi - HeatFlux.*R_W;

%----- Dittus-Boelter verification -----
for i=1:ni+1
if ReL(i) < 10000
```

```
alertR= 'Dittus-Boelter error';
else
alertR = 'OK';
end
end

alertRe =['Reynolds alert:',alertR];

if PrL >= 0.7 && PrL <= 160
alertP= 'OK';
else
alertP = 'Dittus-Boelter error';
end
alertPr =['Prandlt alert:',alertP];

end
```

PRESSURE DROP

```
function [DeltaPres,v] = PDrop(rhoL,m_tot,d,muL,k,x,P_out,ni)
% Pressure drop considering all mass flow as liquid single phase.
% Considering only pressure drop due to friction. Gravity and acceleration
% are not included.

%----- Previous calculations -----
A = pi/4*d.^2;           %[m2] - Pipe inner area
Q = m_tot/rhoL;         %[m3/s] - Volume flow for one-phase (liquid)
v = Q./A ;              %[m/s] - Velocity for one-phase (liquid)

%----- Calculating -----
ReL = rhoL*v.*d./muL;

for i=1:ni+1

if ReL(i) <= 2100
f = 64./ReL;
else
if ReL(i) >= 4000

f = 1./((-1.8*log((6.9./ReL) + (k./(3.75.*d)).^(1.11))).^2);

elseif ReL(i) > 2100 && ReL(i) < 4000

f = 1/2*(64./ReL + 1./((-1.8*log((6.9./ReL) + ...
(k./(3.75.*d)).^(1.11))).^2) );
end
end
end

DeltaP = 1/2.*f.*rhoL.*v.^2.*x./d; %Pressure drop for single phase
P_out = P_out*ones(1,length(x));
DeltaPres = 10.*DeltaP;           %10times to multiphase flow

end
```

FLOW REGIME

```
function [regimeMan, usL, usG, regM, alertM] = FlowRegMan(rhoL,rhoG,...  
alphaL,m_tot,d,ni)
```

```
%----- NOTE: REGIME FORMAT -----  
% NOTE: REGIME FORMAT  
% Stratified & Wavy = 1  
% Slug & Bubble = 2  
% Annular = 3  
% Dispersed = 4  
%-----  
  
%----- Changing values to English Units -----  
% Calculating Superficial Velocities  
usGo = (1-alphaL)* m_tot./ (rhoG*(pi/4.*d.^2));  
usG = usGo /0.3048;  
usLo = alphaL* m_tot./ (rhoL*(pi/4.*d.^2));  
usL = usLo /0.3048;  
  
%----- Estimating parameters to comparison -----  
X = 1; %Estimation without correction factors  
Y = 1;  
  
usL1 = 10^(1.1461)*Y;  
usL2 = 10^(-0.301)*1/Y;  
usL3 = 10.^(-1.2599.*log10(usG)+0.5796)*X;  
usL4 = 10^(-0.5229)*Y;  
usL5 = 10.^(-6.0777.*log10(usG)+9.214)*X;  
usL6 = 10.^(2.197.*log10(usG)-4.0425)*X;  
usL7 = 10.^(4.8658.*log10(usG)-10.346)*X;  
  
usG1 = 10^(1/1.2599* (0.301/(X*Y) + 0.5796));  
usG2 = 10^(1/1.2599* (0.5229*Y/X + 0.5796));  
usG3 = 10^(1/6.0777* (0.5229*Y/X + 9.214));  
usG4 = 10^(1/6.0777* (9.214-(log10(0.01)/X)));  
usG5 = 10^(1/2.197* (1.1461*Y/X + 4.0425));  
  
%----- Calculating -----  
regimeMan = zeros(1,ni+1);  
  
for i=1:ni+1  
if usG(i) <= usG1  
if usL(i) <= usL2  
regimeMan(i) = 1;  
else  
if usL(i) >= usL2 && usL(i) <= usL1  
regimeMan(i) = 2;  
else
```

```

regimeMan(i) = 4;
end
end
else
if usG(i) >= usG1 && usG(i) <= usG2
if usL(i) <= usL3
regimeMan(i) = 1;
else
if usL(i) >= usL3 && usL(i) <= usL1
regimeMan(i) = 2;
else
regimeMan(i) = 4;
end
end
end
else
if usG(i) >= usG2 && usG(i) <= usG3
if usL(i) <= usL4
regimeMan(i) = 1;
else
if usL(i) >= usL4 && usL(i) <= usL1
regimeMan(i) = 2;
else
regimeMan(i) = 4;
end
end
end
else
if usG(i) >= usG3 && usG(i) <= usG4
if usL(i) <= usL5
regimeMan(i) = 1;
else
if usL(i) >= usL5 && usL(i) <= usL6
regimeMan(i) = 3;
else
if usL(i) >= usL6 && usL(i) <= usL1
regimeMan(i) = 2;
else
regimeMan(i) = 4;
end
end
end
end
else
if usG(i) >= usG4 && usG(i) <= usG5
if usL(i) <= usL6
regimeMan(i) = 3;
else
if usL(i) >= usL6 && usL(i) <= usL1
regimeMan(i) = 2;
else
regimeMan(i) = 4;

```

```

end
end
else
if usL(i) <= usL7
regimeMan(i) = 3;
else
regimeMan(i) = 4;
end
end
end
end
end
end
end

if regimeMan == 1
regimeManTxt = 'Stratified & Wavy';
else
if regimeMan == 2
regimeManTxt = 'Slug & Bubble';
else
if regimeMan == 3
regimeManTxt = 'Annular';
elseif regimeMan == 4
regimeManTxt = 'Dispersed';
end
end
end

regM = ['Mandhane regime:', regimeManTxt];

for i=1:ni+1
if usG(i) > 270 || usL(i) > 30
alertMan = 'Out of range';
else
alertMan = 'OK';
end
end

alertM = ['Mandhane alert:', alertMan];

end

```

FLOW REGIME MAP

```
function[usG3,usG5,usG6,usG7,usL1,usL2,usL3,usL4,usL5,usL6,usL7,...  
usG1_1,usG1_2,usG2_1,usG2_2,usG4_1,usG4_2] = RegMapMan(usL,usG)
```

```
X=1;
```

```
Y=1;
```

```
% DATA FOR PLOTTING
```

```
usG1_1 = 0.1;
```

```
usG1_2 = 10^(1/2.197* (1.1461*Y/X + 4.0425));
```

```
usL1 = 10^(1.1461)*Y;
```

```
usG2_1 = 0.1;
```

```
usG2_2 = 10^(1/1.2599* (0.301/(X*Y) + 0.5796));
```

```
usL2 = 10^(-0.301)*1/Y;
```

```
usG3_1 = usG2_2;
```

```
usG3_2 = 10^(1/1.2599* (0.5229*Y/X + 0.5796));
```

```
usG3 = usG3_1:0.1:usG3_2;
```

```
usL3 = 10.^(-1.2599*log10(usG3)+0.5796)*X;
```

```
usG4_1 = usG3_2;
```

```
usG4_2 = 10^(1/6.0777* (0.5229*Y/X + 9.214));
```

```
usL4 = 10^(-0.5229)*Y;
```

```
usG5_1 = usG4_2;
```

```
usG5_2 = 10^(1/6.0777* (9.214-(log10(0.01)/X)));
```

```
usG5 = usG5_1:0.1:usG5_2;
```

```
usL5 = 10.^(-6.0777*log10(usG5)+9.214)*X;
```

```
usG6_1 = usG4_2;
```

```
usG6_2 = usG1_2;
```

```
usG6 = usG6_1:0.1:usG6_2;
```

```
usL6 = 10.^(2.197*log10(usG6)-4.0425)*X;
```

```
usG7_1 = usG1_2;
```

```
usG7_2 = 10^(1/4.8658* (10.346+(log10(30)/X)));
```

```
usG7 = usG7_1:0.1:usG7_2;
```

```
usL7 = 10.^(4.8658*log10(usG7)-10.346)*X;
```

```
end
```

SOLUBILITY

```
function [SolBulk,SolWall,SolubDiff,ConcGrad] = Solubility(Tb,Twi,WAT,ni)
```

```
----- Calculating based on precipitation curve -----
```

```
for i=1:ni+1
```

```
if Tb(i) <= WAT(i)
```

```
%OLGA equation at ^3 WAT 42 C
```

```
BulkSol(i) = -6.618E-8*Tb(i).^3 + 6.290E-5*Tb(i).^2 -...
```

```
1.994E-2*Tb(i) + 2.109 ;
```

```
WallSol(i) = -6.618E-8*Twi(i).^3 + 6.290E-5*Twi(i).^2 -...
```

```
1.994E-2*Twi(i) + 2.109 ;
```

```
Grad(i) = -3*6.618E-8*Tb(i).^2 + 2*6.290E-5*Tb(i) - 1.994E-2 ;
```

```
% %OLGA equation modified at ^3 WAT 35.5 C
```

```
% BulkSol(i) = -6.92E-8*Tb(i).^3 + 6.589E-5*Tb(i).^2 -...
```

```
2.090E-2*Tb(i) + 2.208 ;
```

```
% WallSol(i) = -6.92E-8*Twi(i).^3 + 6.589E-5*Twi(i).^2 -...
```

```
2.090E-2*Twi(i) + 2.208 ;
```

```
% Grad(i) = -3*6.92E-8*Tb(i).^2 + 2*6.589E-5*Tb(i) - 2.090E-2 ;
```

```
----- Changing to solublity curve -----
```

```
BulkSol(i) = 0.043 - BulkSol(i) ;
```

```
WallSol(i) = 0.043 - WallSol(i) ;
```

```
GradSol(i) = Grad(i);
```

```
else
```

```
BulkSol(i) = 0.043;
```

```
WallSol(i) = 0.043;
```

```
end
```

```
end
```

```
SolBulk = BulkSol ;
```

```
SolWall = WallSol ;
```

```
SolubDiff = WallSol - BulkSol;
```

```
ConcGrad = GradSol ;
```

```
end
```

WAX DEPOSITION

```
function [deltaWnew,dnew] = WaxDepo(mwW,rhoW,rhoL,muL,usL,usG,Tb,Twi,...
SolubDiff,h_in,tkL,d,regimeMan,time_step,C1,C2,C3,deltaW,rhoM,ni,ConcGrad)

%----- Previous calculations -----
volW = mwW/rhoW;
deltaW_old = deltaW;
dwax = d ;
muL = muL*1000 ;

%----- Calculating diffusion coefficient -----
Bwc = 7.4e-12;
Dwo = Bwc*mwW^0.5*Tb./(muL*volW^0.6);

%----- Accounting the wax porosity effect -----
Ref = rhoL*usL.*dwax./muL;
Coil = 100*(1-(Ref.^0.15)/8);
Phil = C1./(1-Coil./100);

%----- Accounting the rate reduction -----
usL = usL*0.3048;
usG = usG*0.3048;

uM = usL + usG;
E = 1./(1+(uM/8.66).^1.39);

%----- Calculating Res using Baker map flow regime -----
%----- NOTE: REGIME FORMAT -----
% NOTE: REGIME FORMAT
% Stratified & Wavy = 1
% Slug & Bubble = 2
% Annular = 3
% Dispersed = 4
%-----

Res=zeros(1,ni+1);

for i=1:ni+1
if regimeMan(i) == 1
Res(i) = rhoL.*usL(i).*deltaW(i)./(E(i).*muL);
else
if regimeMan(i) == 2
Res(i) = rhoM.*usL(i).*deltaW(i)./(E(i)*muL);
else
if regimeMan(i) == 3
Res(i) = ((rhoL*rhoM)^0.5).*usL(i).*deltaW(i)./(E(i).*muL);
elseif regimeMan(i) == 4
Res(i) = 0;
end
end
end
end
end
```

```
end  
end  
end  
end
```

```
Phi2 = C2.*Res.^C3;
```

```
%CTG = SolubDiff./(Tb-Twi);  
CTG = ConcGrad
```

```
TRG = (Tb - Twi).*h_in./tkL ;
```

```
deltaW = Phi1./(1+Phi2).*Dwo.*CTG.*TRG*time_step;  
deltaWnew = deltaW + deltaW_old;  
dnew = d-2*deltaW ;
```

```
end
```